
Article:
Yasa, E. orcid.org/0000-0001-5443-3598, Poyraz, O. orcid.org/0000-0001-9892-5738, Molyneux, A. orcid.org/0000-0002-3289-3718 et al. (3 more authors) (2024) Systematic review on additive friction stir deposition: materials, processes, monitoring and modelling. Inventions, 9 (6). 116. ISSN 2411-5134

https://doi.org/10.3390/inventions9060116

---

inventions

MDPI

Review

Systematic Review on Additive Friction Stir Deposition: Materials, Processes, Monitoring and Modelling

Evren Yasa *, Ozgur Poyraz, Anthony Molyneux, Adrian Sharman, Guney Mert Bilgin and James Hughes

AMRC North West, University of Sheffield, Blackburn BB2 7HP, UK; o.poyraz@amrc.co.uk (O.P.); a.molyneux@amrc.co.uk (A.M.); a.sharman@amrc.co.uk (A.S.); g.bilgin@amrc.co.uk (G.M.B.); j.hughes@amrc.co.uk (J.H.)

* Correspondence: e.yasa@sheffield.ac.uk or e.yasa@amrc.co.uk

Abstract: Emerging solid-state additive manufacturing (AM) technologies have recently garnered significant interest because they can prevent the defects that other metal AM processes may have due to sintering or melting. Additive friction stir deposition (AFSD), also known as MELD, is a solid-state AM technology that utilises bar feedstocks as the input material and frictional–deformational heat as the energy source. AFSD offers high deposition rates and is a promising technique for achieving defect-free material properties like wrought aluminium, magnesium, steel, and titanium alloys. While it offers benefits in terms of productivity and material properties, its low technology readiness level prevents widespread adoption. Academics and engineers are conducting research across various subfields to better understand the process parameters, material properties, process monitoring, and modelling of the AFSD technology. Yet, it is also crucial to compile and compare the research findings from past studies on this new technology to gain a comprehensive understanding and pinpoint future research paths. This paper aims to present a comprehensive review of AFSD focusing on process parameters, material properties, monitoring, and modelling. In addition to examining data from existing studies, this paper identifies areas where research is lacking and suggests paths for future research efforts.

Keywords: additive manufacturing; additive friction stir deposition; process modelling; process monitoring

Citation: Yasa, E.; Poyraz, O.; Molyneux, A.; Sharman, A.; Bilgin, G.M.; Hughes, J. Systematic Review on Additive Friction Stir Deposition: Materials, Processes, Monitoring and Modelling. *Inventions* **2024**, *9*, 116. https://doi.org/10.3390/inventions9060116

Academic Editor: Craig E. Banks

Received: 24 September 2024
Revised: 4 November 2024
Accepted: 11 November 2024
Published: 13 November 2024

1. Introduction

The widespread use and industrialisation of metal additive manufacturing (AM) has accelerated in the last decade, with aerospace and biomedical being the leading sectors to adopt these methods [1–3]. Among the various metal AM technologies, two main types have been extensively studied and implemented, namely powder bed fusion (PBF) and directed energy deposition (DED), which are both fusion-based AM technology groups [4]. PBF techniques, such as laser-beam powder bed fusion (PBF-LB) and electron-beam powder bed fusion (PBF-EB), utilise a laser or electron beam to selectively melt and fuse powder particles layer-by-layer. Alternatively, DED methods, such as laser-beam (DED-LB) and electron-beam directed energy deposition (DED-EB) and wire arc additive manufacturing (WAAM), involve feeding material in the form of powder or wire and melting it using an energy source as it is deposited onto the build platform. While these technologies offer high precision and the ability to produce complex geometries, they also present challenges such as the creation of residual stresses, anisotropy in mechanical properties, and the necessity for post-processing [3,4].

Solid-state AM techniques, including additive friction stir deposition (AFSD), have emerged as promising alternatives to traditional fusion-based methods [4]. AFSD involves the mechanical stirring of material to induce high amounts of plastic deformation and bonding at temperatures below the melting point, thereby mitigating many of the issues

associated with melting and solidification [5,6]. In AFSD, a rotating tool is used to stir the material, creating a solid-state bond without melting the base material. This results in a fine-grained microstructure and enhanced mechanical properties, such as increased strength and ductility [4,5]. The process dynamics allow for the creation of large, near-net-shape components with excellent mechanical properties. Studies have demonstrated the effectiveness of AFSD in fabricating components from various materials with applications for aerospace, automotive, and defence industries [7,8]. Compared to fusion-based AM methods, AFSD offers several advantages. These include lower residual stresses, reduced anisotropy, and the ability to join dissimilar materials without the formation of brittle intermetallic phases [3,6]. Moreover, Khodabakhshi et al. [3] and Dilip et al. [5], have shown the significant potential of AFSD in producing parts with superior mechanical properties and reduced defects. AFSD can also be used to repair damaged components, providing a cost-effective solution for extending the life of critical parts [9,10].

AFSD is an emerging AM technology with a low technology readiness level (TRL). Thus, understanding the process–property–performance relations, finding the suitable process windows for different materials, process monitoring and control, and process modelling are new areas of research and development for technology. Although limited work has been carried out in AFSD so far, defects can be detected and mitigated in real-time by monitoring key parameters such as temperature, force, and tool position. This approach leads to improved part quality and reduced scrap rates [11]. Recent studies have highlighted the importance of real-time temperature monitoring and control to achieve consistent material properties and surface quality [12,13]. Additionally, monitoring the force applied by the tool and the torque during the process helps in maintaining optimal and stable process conditions [11,14]. However, the AFSD process still lacks quantitative correlations between process controls and the final microstructure and characteristics [15]. To overcome the challenge, temperature-based monitoring systems have recently gained popularity. Hartley et al. and Griffiths et al. used a digital microscope to conduct the in situ monitoring of substrate distortion and material flow behaviour [16,17]. However, future research efforts are expected to prioritise number of crucial areas such as advancing the fabrication of complex geometries, tailoring material properties, and exploring novel materials by integrating various sensors for in situ monitoring [18].

The modelling of the AFSD process is also crucial for understanding and optimising the complex relations between the tool, material properties, and process parameters. Numerical simulations and analytical models are mostly employed to predict the temperature distribution, material flow, and the mechanical properties of the deposited layers. Zhang et al. developed a finite element model to simulate the temperature field and material flow during AFSD, providing insights into the thermal history and its impact on the obtained mechanical properties [19]. Additionally, process models are essential for scaling up the AFSD process and transferring it to different materials and geometries [20,21].

The properties of the material deposited through AFSD are influenced by several process variables, including layer height, rotational speed, traverse speed, actuator speed, temperature, and feedstock characteristics [22–26]. Ghadimi et al. demonstrated that layer height affects tensile properties, with thinner layers (1 mm) showing lower fracture strains and ultimate tensile strength compared to thicker layers (2 and 3 mm) [24]. The rotational speed of the tool impacts mechanical properties by altering heat input and grain size. Higher rotational speeds generally increase heat input, leading to larger grain sizes and reduced tensile strength and hardness [27]. The traverse speed and feed rate also affect heat input and microstructure [27]. Higher traverse speeds can increase grain sizes and decrease recrystallization, thereby enhancing tensile strength in materials like aluminium alloy 6061 (AA6061) [28]. The characteristics of the feedstock material, such as its tempering condition, play a crucial role in determining process parameters and final material properties [23]. Ahmed et al. illustrated that different temper conditions for AA2011 require different rotational speeds to achieve optimal deposition, resulting in varied mechanical properties [23]. Materials subjected to AFSD typically exhibit fine-grained

microstructures, which enhance mechanical properties such as strength and ductility [3,6,8]. The process also allows for the use of a wide range of materials, including high-strength alloys and composites, which are challenging to process using traditional fusion-based AM techniques [3]. Investigations into aluminium alloys like AA6061 and AA7075 have shown that AFSD can achieve high tensile strengths and elongation values when combined with a post-deposition heat treatment, making it suitable for structural applications [22,29]. Furthermore, the ability to process dissimilar materials without forming brittle intermetallic phases expands the potential applications of AFSD in industries requiring multi-material components [7,30].

AFSD is an emerging AM technology with promising potential, but knowledge gaps still exist. A comprehensive review of the current state of the art is necessary considering the rapidly evolving landscape of AFSD research and development. This paper aims to consolidate the advancements in various research areas of the AFSD process, including process development, process monitoring and control, and process modelling. This paper summarises the most recent research findings, highlighting potential uses of AFSD and suggesting future research directions to address existing challenges to expand its industrial applications. This review aims to serve as a valuable resource for researchers and practitioners in the field, providing a detailed understanding of the AFSD process and its capabilities.

2. Additive Friction Stir Deposition

AFSD is a solid-state metal AM process that exploits the friction stir welding mechanism, combining it with a material feeding system to create fully dense three-dimensional (3D) components in their as-deposited state [11], and at a higher build rate than many other AM processes [18]. The combination of heat and the severe plastic deformation of the deposited material produces components with similar properties to wrought materials without the defects that result from melting and solidification-based processes [31].

The AFSD process, which is currently almost always performed on a CNC cartesian coordinate machine, uses a substrate mechanically mounted on the machine table, as shown in Figure 1. The feedstock, which has a square or circular cross-section, is fed through a rotating tool and pushed towards substrate's top surface vertically via an actuator. As the result of this initial motion, the generated frictional heat causes a localised increase in temperature around the tool. Since the temperature increases, the yield strength of the feedstock material decreases, and material becomes softer and more ductile. With the yield strength reduced, the feedstock material undergoes significant plastic deformation. It then yields and is forced outwards, filling the space between the substrate and rotating tool. As the material is forced outwards, the combined compressive force from the feed mechanism and shearing force from the rotating tool cause the material to plasticise. This rapid plastic deformation results in further volumetric heat generation [13]. The deposited material mixes with the substrate or previous layers as it is plastically deformed and forced into the substrate in the feedstock zone, creating a strong metallurgical bond. The substrate is also heated, softened, and forced upwards into the tool's affected zone, resulting in a strong interface [32]. Once plasticisation is initiated, computer numerically controlled (CNC) in-plane motion is used to deposit material in the desired shape.

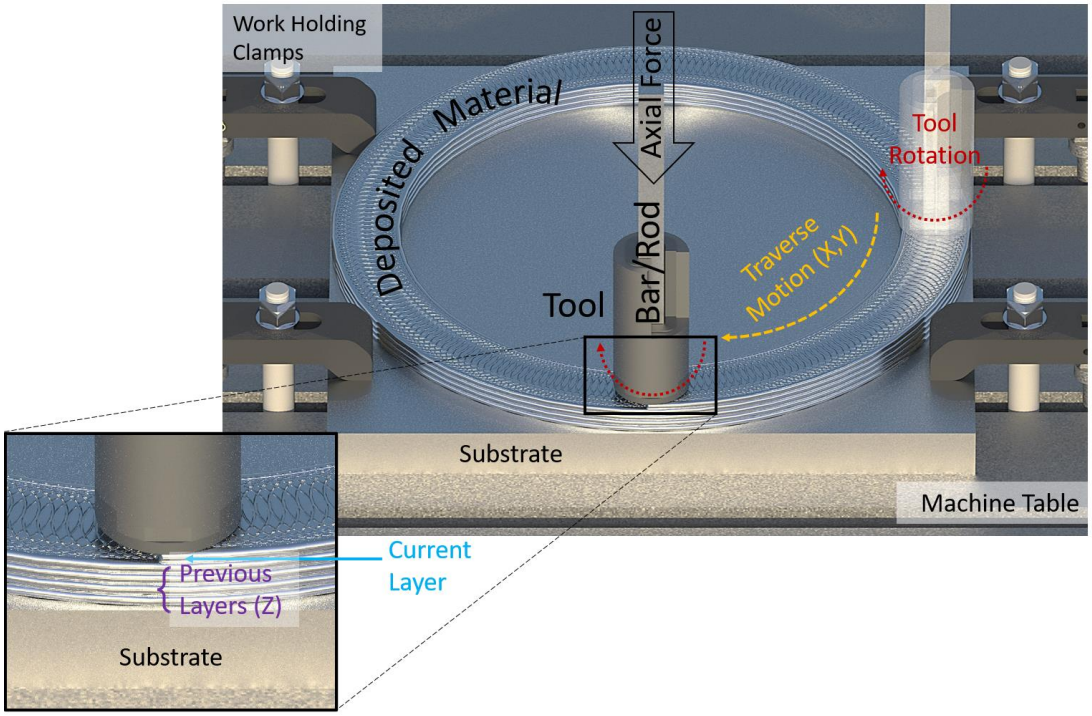

Figure 1. Schematic illustration of the AFSD process.

2.1. AFSD Tools

The tools typically employed for AFSD consist of a robust metal body made of H13 [33] or 40Cr steel [34] to encase the feedstock, rotate it, and withstand the process forces/temperatures. As the AFSD process utilises a rotational motion to introduce a friction between the feedstock and the substrate, the tools' geometries are usually designed with a cylindrical exterior profile [12,22,24]. This cylindrical exterior shape is often paired with a hollow pathway of square or circular shape [21,29,35]. The tool's internal volume can mirror the feedstock's shape closely, with minimal space, to prevent rubbing or friction between the internal face of the tool and the external face of the feedstock. The tool shoulder, which is the bottom flat plane opposite the substrate top surface, might have a gap between 1 and 3 mm to allow the flow of the plasticized material during the rotational and transverse movements [36]. Although the gap between the tool shoulder and substrate's top surface is set to an exact value, the achieved layer thickness may follow a lower value [21]. Jin et al. found that the thickness of the layer was 0.85 mm even though they used a 1 mm gap between the tool shoulder and substrate [21]. Protrusions of different shapes may be present at the bottom of the tool body to aid in stirring materials during the process. Ghadimi et al. employed a deposition tool featuring pairs of teardrop-shaped protrusions on its lower face [24]. Figure 2b illustrates the deposition tool and the detailed structure of the deposited layers, highlighting the significant impact of the tool's design on the AFSD process [24]. These protrusions may play a crucial role in the AFSD process by stirring the softened material and generating additional heat through friction [13]. The presence of these protrusions also allows for the re-stirring of previously deposited layers if the new layer thickness is smaller than the height of the protrusions. Conversely, if the layer thickness exceeds the height of the protrusions, the tool does not interact with the underlying layers. This dynamic interaction between the protrusions and the existing layers or substrate results in a distinct and efficient material deposition pattern, enhancing the overall quality and consistency of the deposited material [13]. Moreover, some tools may include a built-in thermocouple for temperature monitoring and adjusting process inputs (see Figure 2a). These instruments could also be combined with specialised thermocouple collars made of polymer material created using 3D printing techniques [12]. These ring-shaped collars can then be fitted on the exterior cylindrical face of the tool and can

carry more than one thermocouple for enhanced temperature monitoring [12]. As can be understood from the explanations in this section, the tool designs made for AFSD are determined according to the application principles of the process and other additional operations carried out with the process, such as temperature monitoring. In this context, future developments might likely show enhanced tool designs with varied monitoring options embedded in the tool body, such as position, force, or vibration. Thus, it would be useful to follow future developments in AFSD tool design.

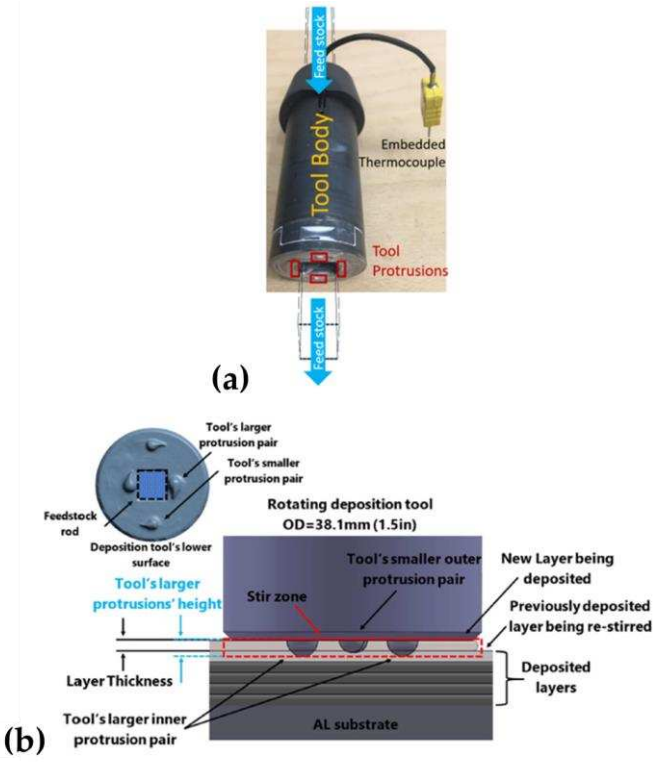

Figure 2. (**a**) Tool overview; (**b**) deposition tool schematics showing protrusion pairs [24].

2.2. Advantages of the AFSD Process

AFSD can process difficult-to-weld or difficult-to-melt materials due to the solid-state nature of the process. Therefore, high-strength alloys which are susceptible to cracking during solidification or reactive materials can be processed without melting them through AFSD. In the open literature, AFSD has been demonstrated to be feasible with aluminium alloys [8–13,21–32], nickel and titanium alloys [37–41], magnesium alloys [42–46], copper alloys [13,17,47], and stainless steels [27]. The relative flexibility of feedstock allows for the use of lower quality materials, including recycled material, without the need for expensive, energy-intensive reprocessing such as gas atomisation to convert material back to powder form. It has been demonstrated that it is possible to directly use loose, unprocessed machine chips to successfully deposit fully dense material [48], albeit using dry cut chips. Otherwise, a cleaning process may be required for chips cut using coolant/cutting fluid. This was demonstrated with AA5083 and a similar study by Agrawal et al. achieved similar results using Ti6Al4V chips [37].

Depending on the material being processed, AFSD can be performed in an open environment without the need for an inert gas environment in a sealed chamber, which can dramatically increase the maximum build volume. This means the process is highly scalable in the same way that CNC milling machines are [49]. This is particularly advantageous when compared to powder bed fusion processes, which are limited in the build volume partially due to the requirement of an inert chamber as well as the significant increase in excess feedstock required to fill a larger build volume. There are some limitations depending on the material being processed. For example, titanium alloys need to be

processed in an inert atmosphere due to their high reactivity, causing oxidation at elevated temperatures [41].

Fusion-based AM with DED and PBF processes produce components with significant residual stresses [50,51] which can require extra post-processing steps to remove. AFSD is generally considered to produce lower residual stress than fusion-based processes [11]; however, residual stress does still occur [52]. Zhu N. et al. showed that stresses produced were still significant, even in a low yield strength, such as that of a deposited material like AA6061 [53]. They also showed that residual stresses are not evenly distributed over the entirety of the component, with different residual stresses experienced at the start of deposition tracks compared to the ends, as well as differing stresses at different heights of deposition [53]. This is logical, as the layers closer to the substrate experience a raised temperature for longer than layers nearer to the top of a component. The presence of this residual stress should be taken into account when designing large parts for the process; even though maximum build size is not limited by the process itself, residual stresses may make work holding a problem due to substrate warping.

2.3. Limitations of the AFSD Process

AFSD is a near-net shape process and the achieved in-plane resolution is very low compared to other AM processes such as PBF-LB, limited to approximately 10 mm or higher depending on the tool and feedstock geometry [54]. Components also have a poor surface quality and machining is almost always needed, as demonstrated by the wall geometry in Figure 3. The poor surface quality on the side walls is primarily caused by flash, which forms as excess material is forced out beyond the deposition zone of the tool. This causes weak bonds between layers at the edges of the deposited track, where the flash is not mixed with previously deposited material or substrate [49].

Figure 3. A single-track wall manufactured by AFSD in AA6xxx series.

The top surface may also suffer from poor quality in the form of a regular ring pattern known as onion skin, as well as a very rough area where the deposition ends and the tool retracts. This effect, known as "the onion skin", shown in Figure 4, is very characteristic to this process, like fish scale in welding or chevrons in LPBF. The pitch of the onion skin pattern is calculated to be equal to the advance per revolution of the tool, which suggests that it is caused by the interaction between deposited material and the edge of the tool as it rotates [32]. Moreover, as the severity of the onion skin effect increases due to the uneven spacing or even breakdown of this pattern, a macroscopic defect known as "galling" can be observed. Beading is another process phenomenon, in which excess material forms raised areas on the surface as a result of uneven material flow, insufficient heat control,

or inaccurate tool speed, resulting in a rough surface finish and potential dimensional inaccuracies. It can be mitigated by adjusting process parameters or performing post-processing [49]. Undesired local melting or poor bonding are other defects that may occur in AFSD, mainly due to the improper construction of process parameters. As a result of insufficient material mixing and flow, poor bonding or even delamination can be observed. Additionally, delamination from the substrate may be more pronounced after heat treatment. Thus, it is very critical to construct the process window suitably, leading to defect-free deposition. The construction of process windows is easier for some alloys, such as AA6xxx series, whereas other alloys have a much more limited process window, making the process development harder.

Figure 4. Onion skin observed on the top surface of a deposition.

3. Additive Friction Stir Deposition Process Parameters

Almost all defects in AFSD stem from poorly constructed process windows. Thus, it is very important to understand the effect of each process variable on the obtained quality. The number of variables in AFSD is limited compared to other AM processes, such as LPBF, but various process variables, including the layer height [24], rotational speed [25], traverse speed [22], and actuator speed (or actuator feed rate) [37], still affect the obtained material properties.

The layer height is a value pre-set when the deposition path is planned and generally set to a value between 1 and 2 mm. Yet, there are some studies in the literature experimenting with higher layer thicknesses. Ghadimi et al. showed that layer height affects the tensile properties of the deposited material in the build direction, with the thinnest layer tested (1 mm) having considerably low fracture strains and ultimate tensile strength when compared to specimens built with 2 and 3 mm of layer thickness [24]. There was a negligible difference in the specimens extracted from XY axis. This may be due to an increased likelihood of defects at the layer interfaces; thinner layers effectively have more layer interfaces in the build direction than thicker layers, increasing the prevalence of interface defects. This indicates that it is beneficial to use thicker layers over very thin layers, which may also have the benefit of shorter build times. There is a limit to the maximum layer thickness before mechanical properties are detrimentally affected, due to less mixing with previous layers as the layer height increases.

The rotational speed of the tool or spindle speed is a fundamental parameter of AFSD and has been shown to greatly affect the final mechanical properties of the deposited material. Tool rotation affects the temperature of the plasticised material with a higher rotational speed resulting in higher heat input, which can affect the mechanical properties by increasing grain size [27]. The rotational speed also affects the spindle torque and actuator force, defined as the force required to push the feed rod downward through the tool. These values can be taken as process signatures for AFSD, among others, such as the

temperatures reached in the feedstock or deposited material. In a study conducted with AISI 316L stainless steel, it was shown that the measured actuator force and spindle torque decreased with tool rotational speed (in the range of 400–800 rpm) for a constant feed rate of feed rod and tool traverse speed [15]. Tang et al. showed that a higher rotational speed (600 rpm) resulted in a lower tensile strength and hardness than components produced at the lower speed (400 rpm) [55]. This maybe a result of the higher temperatures reached at high rotational speed, which may be similar to having an in situ heat treatment effect on the component [55]. Ahmed et al. also demonstrated the same effect, with their depositions produced with a lower rotational speed (200 rpm) having a higher hardness than the higher spindle speed (1200 rpm) component [23].

Another parameter that affects the given heat input is the tool traverse speed [27]. It is observed that the change in the traverse speed, also known as feed rate (not to be confused with material feed rate or actuator speed), leads to changes in the microstructure. An increase in the traverse speed increases the grain size and decreases the degree of recrystallization, leading to an increase in the tensile strength for AA6061-T6 [28].

Actuator speed (F), also known as actuator feed rate, is crucial for the interfacial bonding, porosity, and microstructure of the deposit [37]. The feedstock feed rate is controlled by a linear actuator that applies force at the top of the feedstock. This force is nonlinear because the feedstock's elastic modulus and shear behaviour change with increasing temperature near the interaction zone. Thus, as the feedstock is heated and plasticized, the required force at the deposition zone for a given feed rate varies [54]. Williams et al. fabricated AA7020 components at different building rates by adjusting the traverse rate, deposition rate, and actuator feed rate. They used three different actuator feed rate values of 50.4, 101.6, and 254 mm/min, corresponding to slow, medium, and fast building speeds, respectively. It was clear that the slow build produced considerably more flash compared to the medium and fast builds. The slow build also resulted in the lowest deposition efficiency at 56.9%, whereas the medium and fast builds achieved deposition efficiencies of 73.3% and 81.3%, respectively [33]. Researchers at University of Sheffield, AMRC North West attained a comparable outcome when working with Al6061 aluminium alloy on the MELD L3 machine. By keeping all process parameters constant, but lowering the feed rate override (FRO) to 50% (using only half of the set actuator speed), there was an increase in flash formation and also a decrease in productivity (see Figure 5).

Figure 5. Influences of feed rate override (FRO) on flash formation during AA6061 AFSD process under constant rotational speed.

The deposition ratio refers to the relationship between the amount of material deposited during the process and the amount of material originally fed into the system. It

is a measure of the efficiency of the deposition process and is generally expressed as a percentage [4]. Increasing the deposition ratio leads to improvement in productivity, but it may result in poorer surface finish and potential defects such as porosity. Decreasing the deposition ratio enhances surface quality and accuracy while increasing energy consumption [4]. Although not a process parameter, the feedstock material characteristics are also important process inputs leading to changes in the processability and obtained material properties. It has been indicated that feedstock dimensional accuracy, size, shape, and material composition significantly affect the process [3,56]. The feedstock temper condition also has a predominant effect on the process and necessitates changing the processing parameters required to successfully deposit defect-free material. Ahmed et al. showed this in AA2011 using two temper conditions, AA2011-T6 (solution annealed + aged) and AA2011-O (annealed only) [23]. The T6 condition parameters did not work with the O-condition material. T6-treated material required a rotational speed of 1200 rpm, while the O-treated material needed a much lower rotational speed of 200 rpm. This variation in the process parameters leads to different mechanical properties, with the O-treated material having a higher hardness in the as-deposited sample. These finding suggest that although there is some limited flexibility in material feedstock for the AFSD process, the temper condition should be considered when optimising process parameters for a particular temper condition, which will likely result in inferior final part properties if used with another temper condition feedstock.

Process parameters can vary significantly between different materials, as demonstrated in Table 1. Note that these may not necessarily be the optimised parameters but have been shown to successfully deposit these materials.

Table 1. Process parameters for various materials compiled from literature.

Alloy Group	Alloy	Layer Height (mm)	Spindle Speed (rpm)	Traverse Speed (mm/min)	Actuator Speed (mm/min)	Deposition Ratio	Feedstock Size (mm)	Tool Type	Ref.
Aluminium	AA6061	2	300	152.4	127	1.20	9.5	Protrusions 2 mm	[24]
	AA7075	1	275	127	69.9	1.82	9.5	Protrusions 2 mm	[57]
	AA7050	2.75	350	76.2	76.2	1.00	9.5	Flat	[58]
	AA2019	1	200	101.6	88.9	1.14	9.5	Protrusions	[59]
	AA2024	1	300	120	51	2.35		Protrusions 1.5 mm	[32]
	Al-8Ce-10 Mg	1	250	254	152.4	1.67	9.5	Protrusions 2 mm	[60]
Steel	AISI 316	0.5	400	253.8	25.2	10.07	9.5	Flat	[27]
	AISI 316L	0.5	440	2.5	25	0.10	10	Not given	[61]
Titanium	Ti6Al4V	0.5	400	202.8	89.4	2.27	Not given	Not given	[41]
Nickel	Inconel 625	0.5	600	76.2	16.2	4.70	9.5	Flat	[38]
Magnesium	WE43	1	325	152.4	63.5	2.40	9.5	Protrusions 2 mm	[42]
	GW83K	~2.4	300	100	Force Controlled (10 kN)		20	Protrusions 2.5 mm	[43]

4. Additive Friction Stir Deposition Process Monitoring

It is essential to monitor the effect of the combination of process parameters discussed in the previous section on the deposited product to determine the outcome of the AFSD method. The real-time tracking and modification of parameters through process monitoring

techniques are also crucial for identifying any process anomalies during deposition and maintaining optimal in situ process variables [18]. Continuous monitoring ensures consistent part quality, prevents defects, and enhances the overall efficiency and reliability of the AFSD process. Actuator force, spindle torque, material flow dynamics, and temperature distribution on the tool and deposited material/substrate are a few of the parameters that can be monitored during the AFSD process [62].

Effective in situ monitoring techniques, particularly temperature control and material flow analysis, are critical for optimising the process and improving the performance of the deposited product. In situ sensors such as thermal imaging cameras, pyrometers, and embedded thermocouples provide critical data on temperature evolution [13,63], while force sensors and torque transducers offer insights into the mechanical aspects of the process [12]. Additionally, advanced imaging techniques can be used to observe material flow and deformation, further contributing to the optimisation and control of the AFSD process [11,64]. Figure 6 shows the relations between the process inputs and outputs as well as the signatures of the AFSD process. While temperature evolution has received the most attention, there are other process signatures that can be used as control factors for ensuring high product quality, such as actuator force or torque.

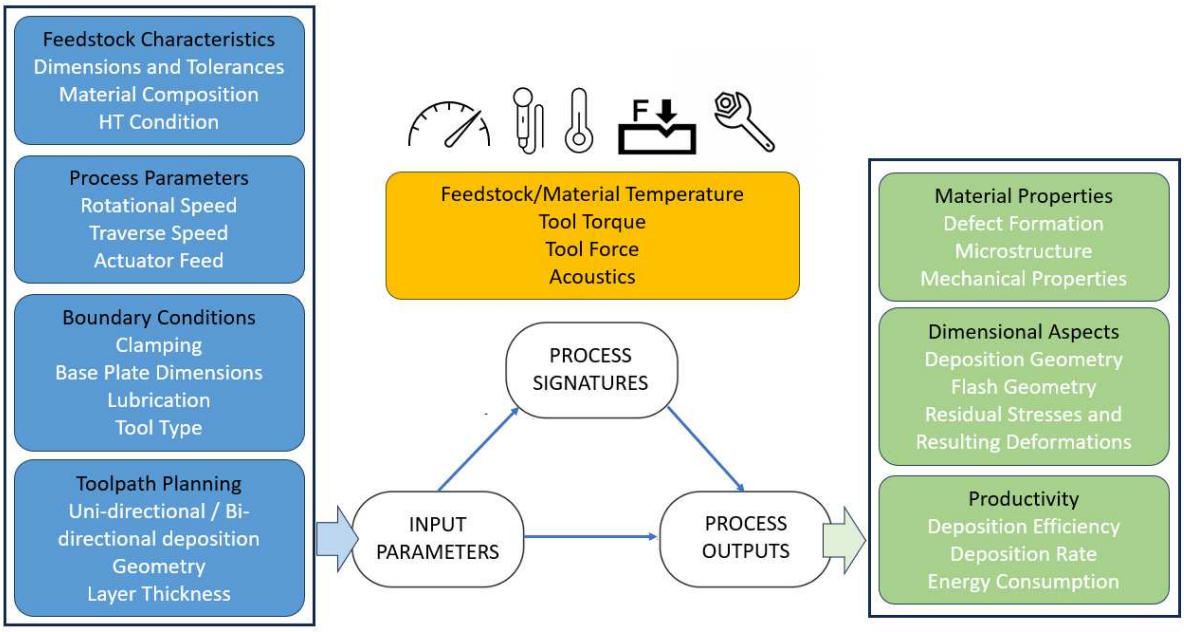

Figure 6. AFSD process showing the relationship between the main input parameters, process signatures, and process outputs based on the literature survey.

The temperature developed in the deposited material during the process is an important process signature, directly influencing the resulting surface quality and defect formation, such as galling and beading [12]. Merrit et al. eliminated these defects by using a closed loop system that measures the tool temperature and adjusts the spindle speed in real time to maintain a set temperature [12]. They showed that the spindle speed reaches steady state at a value close to their minimum set spindle speed of 150 rpm (for AA6061), which is lower than the value typically used in fixed spindle speed studies. The constant temperature resulted in a consistent part finish with no surface defects, which may indicate that it may be more beneficial to control temperature rather than using a fixed spindle speed. A fixed spindle speed may result in an increasing deposition temperature at higher speeds typically used in fixed rpm studies.

Garcia et al. investigated the thermal characteristics of the AFSD process for AA6061 and commercially pure Cu by measuring peak temperatures, exposure times, and reheating/cooling rates [13]. An infrared camera and embedded K-type thermocouples were used to monitor temperatures, while material flow was tracked via optical imaging from

the deposit's leading edge; Figure 7a illustrates these in situ monitoring systems. Garcia et al. found that peak temperatures ranged up to 90% of the melting point, with an average exposure time of 101 s, a reheating rate of 10^2 K/s, and a cooling rate of 10^1 K/s. The study revealed that Cu and AA6061 exhibited different peak temperature relationships with processing parameters due to their distinct material flow behaviours. Accordingly, Cu (Figure 7b) remained stationary while AA6061 (see Figure 7c) deformed significantly, affecting heat generation. This difference was attributed to the materials' varied interfacial contact conditions and flow characteristics [13].

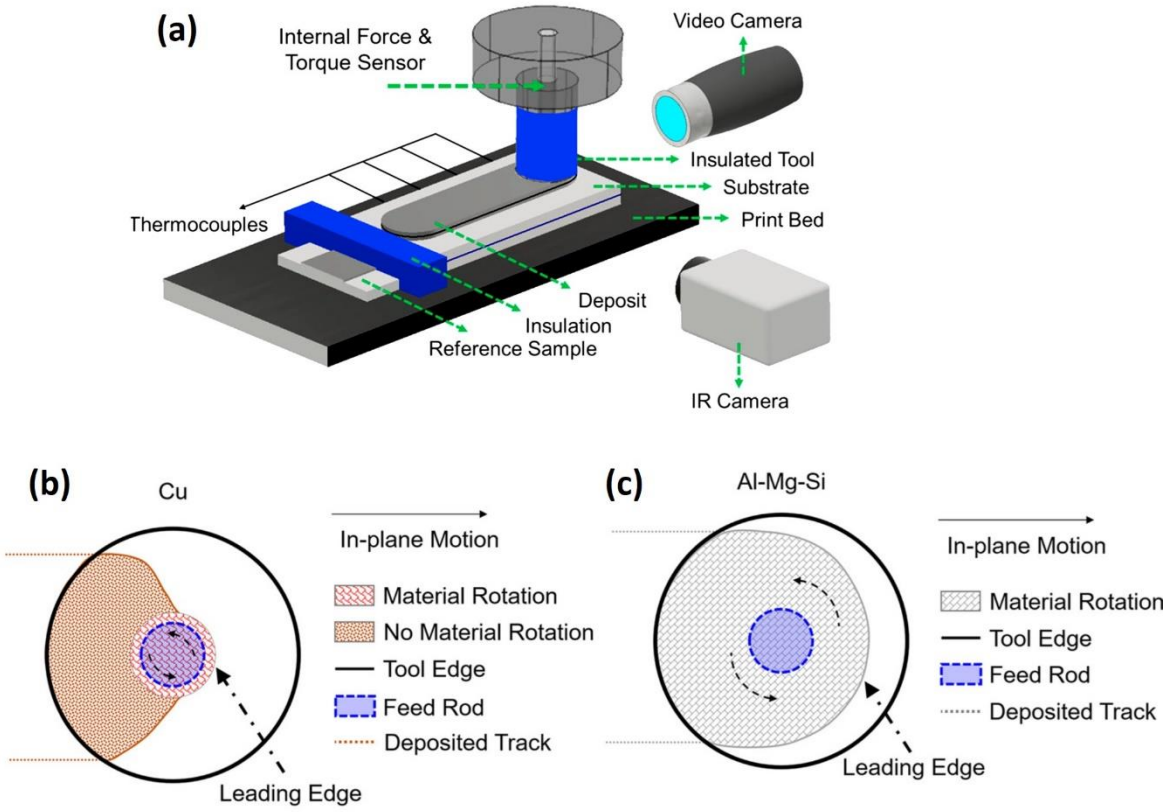

Figure 7. (**a**) An illustration of the in situ monitoring system consisting of infrared and video cameras. The material flow behaviours of (**b**) Cu and (**c**) AA6061 [13].

The study reported by Garcia et al. successfully provided insight into material deformation and flow dynamics on the external surface [13]. However, material flow findings reported by Garcia et al. do not provide an extensive overview of the deformation history of the deposited material, particularly in terms of individual unit deformation during both initial material feeding and steady-state deposition [11]. To address this challenge, Yu et al. offered a potential approach that involves the insertion of tracer material within the feed rod. This approach allowed for the investigation of tracer shape evolution at different stages of AFSD [11]. Moreover, to achieve a comprehensive strain-versus-time relationship at incremental steps during AFSD, X-ray computer tomography emerged as a promising tool, as it was previously used in friction stir welding (FSW) [64].

Some studies on the process monitoring stem from the need to validate the process models developed for the AFSD process. Zhang et al. investigated an integrated finite element model employing the Monte Carlo approach and a precipitate evaluation model based on the temperature field in AFSD of AA6061 [19]. The temperature was determined in situ by using an infrared radiation imaging equipment. The experimental results (the maximum temperature of the first layer was 392.4 °C) were very close to the temperature results obtained from the developed model (390.7 °C). This research served as an outline for

subsequent simulations aimed at understanding microstructural changes and mechanical properties [19].

Merritt et al. implemented in situ monitoring and control during AFSD using thermocouples for temperature feedback and motor current analysis for force feedback, as depicted in Figure 8 [12]. Their experimental setup involved temperature control, force control, and combined temperature and force control procedures during processing AA6061. Force control alone resulted in a tracking error of 130.8 ± 187.7 N, while temperature control alone had a 6.9 ± 5.0 °C, with limited cooling efficiency due to the high heat capacity of the tool and build plate. The combined temperature and force control showed larger temperature errors, primarily because the temperature controller could only passively cool the build, which often saturates the spindle speed at its lowest value. This study highlights the need for more accurate dynamic models to improve closed-loop control in AFSD [12].

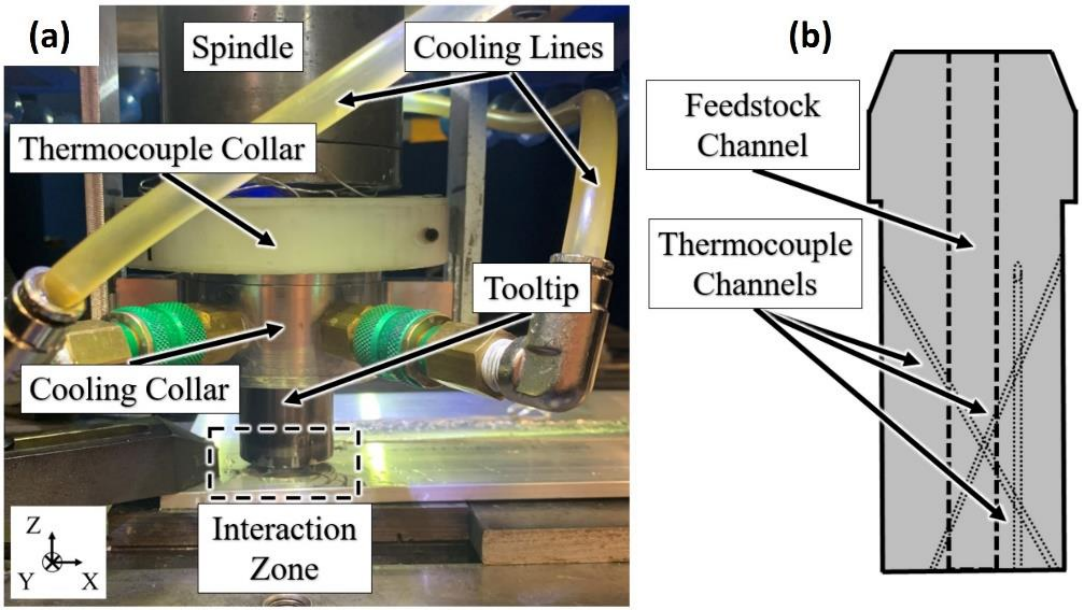

Figure 8. The modified setup showing (**a**) thermocouple and cooling collars, and (**b**) thermocouple channels (licenced under CC BY 4.0) [12].

Chaudhary et al. also proposed a closed-loop control system designed to manage the temperature during the AFSD processing of AA6061 [65]. To reduce the thermal gradient along the build direction, an in situ temperature-controlled system was used to keep the deposition temperature minimum. In addition, the highest temperature during deposition was continually measured with a pyrometer and a thermal imaging camera [65]. Their findings revealed distinct thermal behaviours, as follows: without any external heat source, as shown in Figure 9a, the temperature initially increased due to the friction between the tool and substrate. It peaked and subsequently returned to the room temperature as the tool moved away from the measurement point. Conversely, in the presence of an external heat source, the temperature was kept at a minimum value until it gradually returned to the room temperature, as demonstrated in Figure 9b. This disparity in temperature profiles resulted in considerable variations in the quality of single-layer depositions, as seen in Figure 9c,d [65]. Lower deposition temperatures were clearly related with lower surface quality, as evidenced by the increased occurrence of flashes including accumulated particles in the deposition. In contrast, higher temperatures cause the production of continuous deposition layers with increased surface quality, as depicted in Figure 9d. This improvement is related to the increased material flowability observed at higher temperatures [13]. Moreover, it is shown here that the temperature regulation during deposition in AFSD technique is critical for the obtained part quality [66].

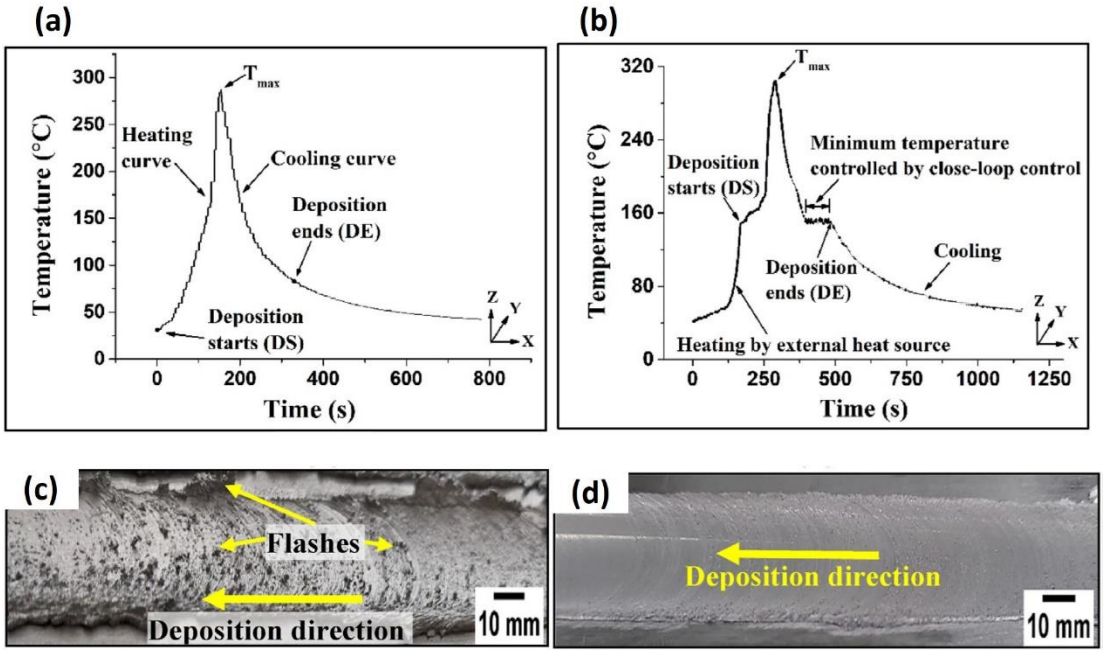

Figure 9. Temperature profile in the experiment (**a**) without an external heat source and (**b**) with a heat source. An image of the deposition (**c**) without an external heat source and (**d**) with a heat source experiments (licenced under CC BY 4.0) [65].

Directly measuring the temperature evolution within the deposited material in AFSD elicits the same challenges as those experienced in FSW and friction stir processing (FSP) [67]. Notably, integrating thermocouples into the processing zone presents difficulties due to the extensive plastic deformation, which could compromise the integrity of physical sensors [14,68]. Furthermore, the presence of the tool in FSW, FSP, and AFSD obscures the stir and deposition zone, preventing the monitoring of temperature evolution, particularly along the normal direction [13]. The position of the deposited material above the substrate distinguishes AFSD from FSW or FSP, in which the stir zone is interior of the workpiece material. As a result, AFSD has the benefit of allowing temperature measurement in the deposited material using non-contact methods from a lateral perspective utilising equipment like infrared cameras or pyrometers [13,63]. The variations in temperature that occur during AFSD have a significant impact on build quality, microstructural features, and as-built material properties. It is noteworthy that investigating fluctuations in temperature in AFSD also requires an in-depth knowledge of material flow dynamics [13].

Non-contact methods like infrared cameras have been more successful than in-contact measuring methods due to the challenging environment caused by extensive plastic deformation and the presence of the tool [13,63]. Although Garcia et al. and Merritt et al. provided comprehensive insights into the thermal characteristics of AFSD, their findings primarily focused on external surface deformations, leaving gaps in understanding the complete deformation history of deposited materials [11]. Previous researchers proposed using tracer materials and advanced imaging techniques like X-ray tomography for a more detailed analysis of material flow during AFSD [11,64,69,70]. Efforts to validate process models through in situ measurements, as shown by Zhang et al. and Merritt et al., have highlighted the need for more accurate dynamic models to further enhance closed-loop control systems [12,19]. Although temperature-based monitoring systems have become more prevalent, a comprehensive understanding of the relationship between the process controls and the final microstructure and characteristics remains lacking [15]. Future research should prioritise advancing the fabrication of complex geometries, improving resolution, tailoring material properties, and integrating various sensors for comprehensive in situ monitoring [18].

5. Process Modelling of Additive Friction Stir Deposition

Modelling the AFSD process presents numerous advantages to engineers and researchers, especially given the current challenges and limited understanding of this emerging additive manufacturing process. Some key benefits include identifying optimal process parameters to achieve desired part properties, avoiding or minimising the trial-and-error approach and thus saving time and resources, preventing potential defects such as voids, cracks, and stresses, and expediting the development of new alloys tailored to AFSD [71]. Furthermore, modelling and simulations can reveal temperature profiles during the process, which is crucial for controlling the thermal cycles that affect the final properties of the deposited material. Another additional gain from modelling might be to utilise energy-efficient process parameters and to contribute more to sustainable manufacturing practices.

Since AFSD is a relatively new AM process, there are only a few modelling studies that exist in the current state of the art [19,29,72]. Yet, tracing pioneering modelling efforts for the FSW process can provide valuable insights for modelling AFSD, given the similarities in the underlying process physics. For a systematic review of the current state of the art, the classification of different modelling techniques and scales may give useful information for choosing the right modelling approach, considering the complexity, applicability, and computational efficiency of simulations. Figure 10 shows the classification of modelling techniques. In Figure 10, black coloured texts show advantages and red coloured texts show disadvantages of each modelling technique.

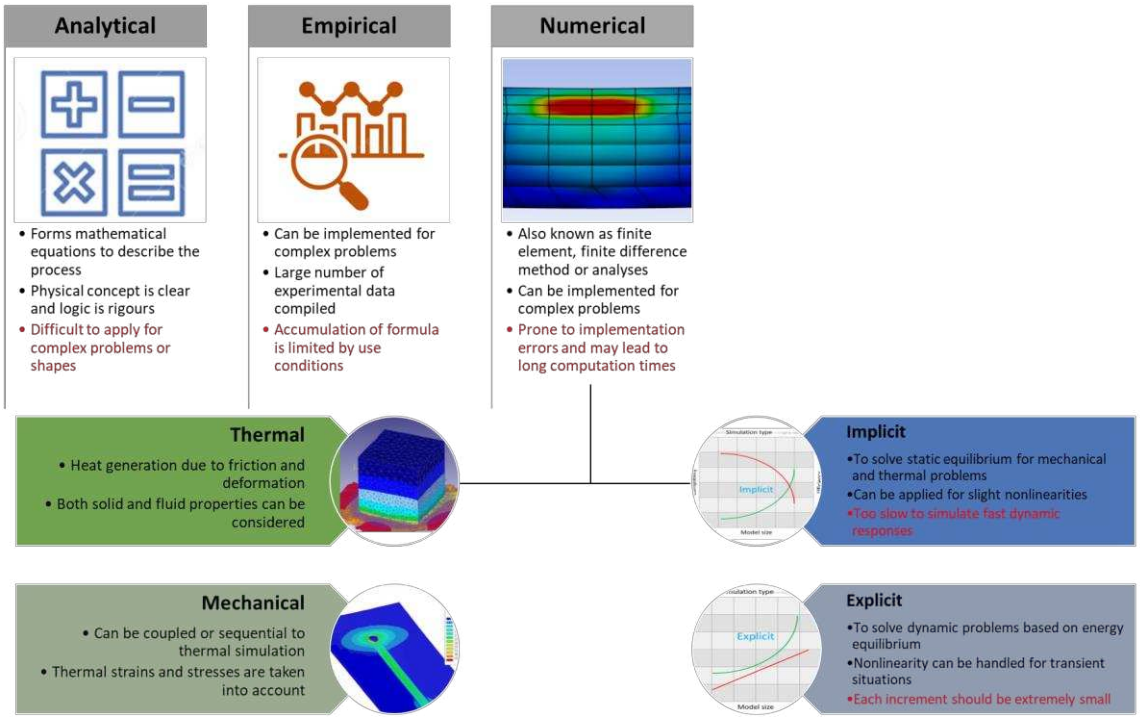

Figure 10. The classification of modelling techniques for the AFSD process.

Analytical models use mathematical equations to describe the physical phenomena involved in the process, and they offer low-to-medium complexity together with fast computation opportunity. They are suitable for initial approximations and understanding fundamental aspects of processes. On the contrary, empirical models can be implemented for complex problems via the compilation of a large volume of experimental data. The trends extracted from the experimental data then can be interpolated or extrapolated to predict the outcomes of the process with different parameter levels. However, the accumulated formulae of the empirical models are limited by use/boundary conditions and cannot directly be applied to different situations. Lastly, numerical methods, which are also

known as methods based on finite element method (FEM) or finite element analyses (FEA), may be implemented for complex problems. Although these are suitable for detailed and accurate predictions of process behaviour, including transient effects, their computational efficiency is low to moderate. Researchers might follow a combined approach to deal with the drawbacks of different modelling techniques, such as introducing analytical equations to thermal models and applying these as boundary conditions in numerical solvers to predict the temperature distribution on a complex shape [73,74]. This hybrid strategy allows for higher accuracy and efficiency, particularly for complex processes like AFSD. Numerical models can also target different problems like those that are thermal or mechanical. While the thermal simulations are established to determine heat generation due to friction or deformation, mechanical models can consider strains and stresses. These two models can also be implemented in a coupled or sequential manner.

One of the pioneering efforts to combine analytical and numerical modelling efforts was presented by Frigaard et al. to predict the heat generation during FSW [75]. In their study, they explained power q_0(W) as a function of pressure P(Pa), tool radius R(m), rotational speed of the tool N(1/s), and friction coefficient μ. They implemented the analytical formula in Equation (1) and solved it with a numerical Matlab 5.2 code [75].

$$q_0 = \frac{4}{3}\pi^2 \mu P N R^3 \quad (1)$$

Although Frigaard et al. reported good agreement between the simulation and experimental temperature values using their approach to employ frictional heating [75], other researchers like Colegrove combined frictional heating and deformation heating and claimed improved convergence between simulation and experimental results [76]. Again, combining analytical and numerical methods, Colegrove accomplished the simulations by introducing further variables like average yield strength and material velocity, as well as the angle between the material flow and traverse vector [76]. This approach was later adopted by researchers such as Song and Kovacevic to ensure the contribution of deformations to heat generation is not underestimated [77].

The modelling efforts were expanded to include computational fluid dynamics (CFD) to model the problem domain with an Eulerian solver using the finite volume rather than the traditional finite element meshes [78]. Different solvers like Lagrangian, Eulerian, or Arbitrary Lagrangian Eulerian (ALE) can handle mesh deformation in various ways (see Figure 11). In Figure 11, red circles show material coordinates while grey squares for nodes and white squares illustrate initial position of the elements and green shadings show the deformed status of the material. The Lagrangian formulation allows for anisotropic material properties to be unaffected by the material's current spatial orientation. This is particularly useful for structural mechanics and other areas of physics that involve a solid material experiencing gradual deformation, which may be anisotropic. If the emphasis is on recreating the physical condition at specific locations in space, an Eulerian expression is typically more practical. Especially with liquids and gases, it is often not feasible to monitor the condition of each individual particle. Conversely, an inherent issue with the pure Eulerian formulation is its inability to accommodate moving domain boundaries, due to physical limitations. That is why it is often preferred to use ALE solutions when it comes to modelling of friction-based processes. Further efforts by Guerdoux combined the accuracy of Lagrangian method with the efficiency of Eulerian method to simulate the whole FSW process [79]. The same solution methods were also practised using other commercial software suites [80].

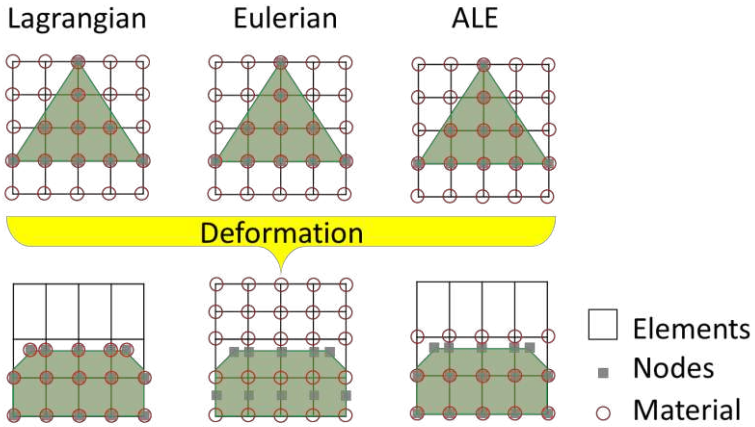

Figure 11. Deformation using Lagrangian, Eulerian, and ALE solvers.

Even though FSW simulations achieved a certain level of computational efficiency and robustness, research on process modelling for the AFSD is still ongoing. The complexity of the process due to layer addition and generation of 3D shapes is an added challenge for this process. Mendieta et al. [29] conducted a study using AFSD modelling on AA6061-T6, which is commonly used in aerospace applications. They attempted to validate their modelling research by comparing the remaining outcomes with experimental data obtained using the contour method. The obstacles in computation, such as simulation times, were addressed by using either an uncoupled or sequential method. While they simulated the initial friction stir process individually, they utilised the resulting strains from this to predict the remaining stresses in the sample [29]. Zhang et al. [19] adopted a moving heat source model for temperature predictions and compared the outcomes with experimental results. They simplified the heat source in their research by introducing a heat fraction flow coefficient between the tool and substrate to represent surface heat input. They also used an AA6061-T6 alloy for manufacturing the specimens and measured the temperatures with the help of infrared radiation image. They reported peak temperatures starting from approximately 400 °C for the initial movement and going down to 300 °C for consecutive layers. Some other research groups introduced meshfree approaches using Smoothed Particle Hydrodynamics (SPH) as a computationally efficient method [20,72]. In the scope of meshfree SPH method, a smooth hyperbolic kernel function, as shown in Figure 12a, was introduced to include the material properties and their interactions with each other. In this manner, the Newtonian hydrodynamics governing the equations were solved in a Lagrangian manner (see Figure 12b) [20]. By this way, more accurate temperature predictions were claimed. The reported temperature values for AA6061-T6 varied between 300 and 525 °C [20].

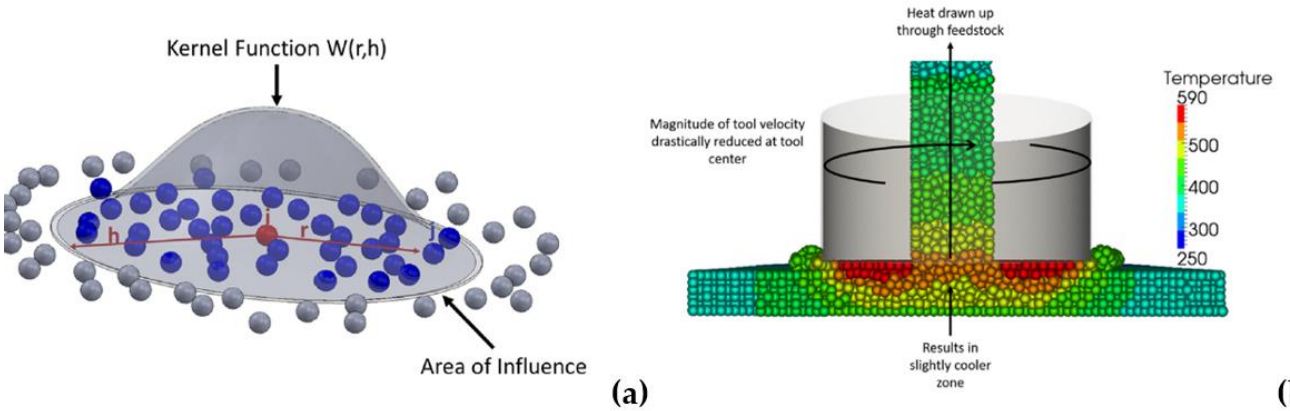

Figure 12. (**a**) Kernel function; (**b**) particle simulation by Stubbfield et al. (under CC BY 4.0 licence) [20].

It is evident from the literature that there are fewer studies on AFSD modelling compared to studies on process-parameter development and material/metallurgical investigations. Nevertheless, there are numerous modelling studies in the literature that focus on FSW as a similar method and some AFSD modelling publications also incorporate FSW principles into their approach [19]. Despite being technically possible, the layered nature of AFSD and the resulting 3D part shapes require more mesh elements, leading to lengthier, less efficient, and more costly simulations [20,72]. Although some researchers value the novel approach of utilising Smoothed Particle Hydrodynamics (SPH) to decrease simulation times, the requirement for sophisticated multi-physics software and intricate pre-processing procedures could hinder its use in regular and everyday simulations. In this aspect, it is important to fill this research gap in the future and introduce more reliable methods or software packages similar to those used for powder bed fusion additive manufacturing.

6. Additive Friction Stir Deposition Metallurgy

In AFSD, strong metallurgical bonding is achieved between the various layers due to the combination of high shear and severe plastic deformation induced by the rotating feedstock being forced into the substrate or previously deposited layer. As previously stated, the peak temperature developed in AFSD is around 60–90% of the materials' melting point and, due to the lack of melting, the issues typically seen with fusion-based AM processes such as porosity, cracking, and elemental segregation are generally avoided when the correct process windows are employed. The microstructure undergoes dynamic recrystallisation, producing a highly refined microstructure with a much smaller grain size than the feedstock material [30,81]. The interface between the deposited material and the substrate typically shows a bowl-shaped depression centred on the feedstock, caused by the interaction of the feedstock driving into the substrate and the substrate material mixing in the shear zone caused by tool rotation [32]. This effect is also demonstrated in Figure 13, showing the microstructure obtained in a study by researchers at University of Sheffield, AMRC North West.

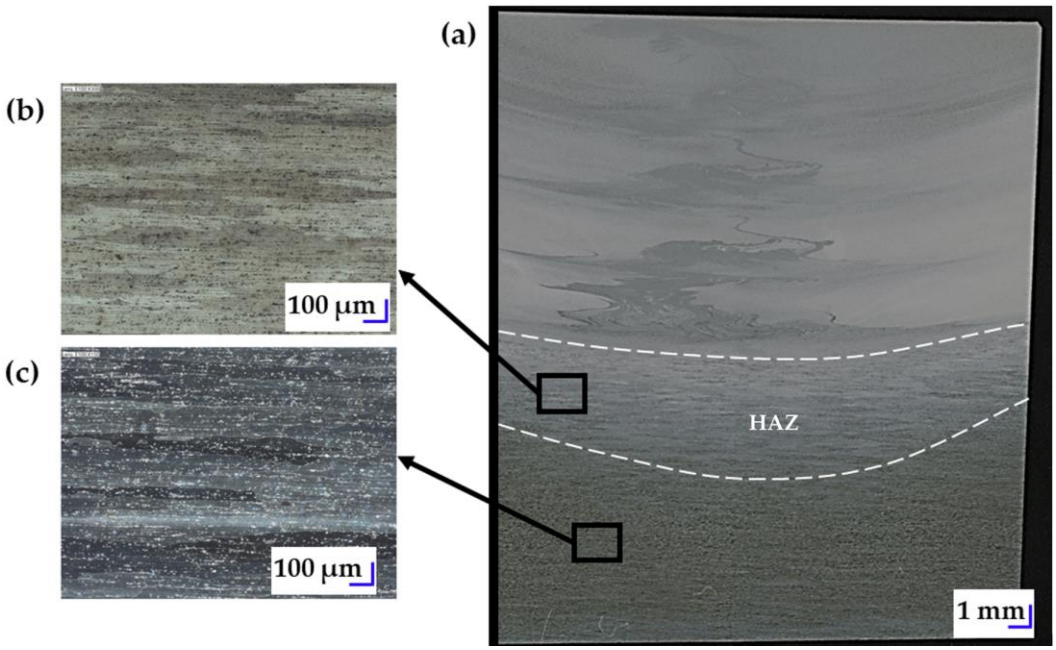

Figure 13. (**a**) Typical bowl-shaped depression centre and the substrate-material mixing in the shear zone caused by tool rotations. (**b**) Image of the heat effected zone, and (**c**) image of the base plate.

In AFSD, aluminium alloys are by far the most studied alloy group, with a range of alloys and metal matrix composites being investigated. AFSD is particularly attractive to high-strength aluminium alloys due to the fact they typically suffer from hot cracking

in fusion-based additive manufacture, and therefore most of the work reported has been conducted on AA6xxx, AA7xxx and AA2xxx series alloys. The microstructure obtained from fusion-based AM typically consists of highly oriented columnar grains resulting from the high thermal gradient produced by the layer-by-layer deposition process. In contrast, all studies of AFSD have shown the microstructure to be equiaxed and highly grain-refined due to the combination of high strain and elevated temperatures. Rivera et al. [82], in a study on AA2219-T851, reported that the feedstock material had a grain size of 30 μm compared to the deposited materials of 2.5 μm, and Perry et al. found that for AA2024 the grain size had reduced to 4.9 μm, compared to the elongated drawn grain structure of the feedstock, which had an average grain size of 57 μm [32]. Rivera et al. also found that no θ′ precipitates were seen in the microstructure, suggesting that the temperature generated was above the solvus and the cooling rate long enough that large θ particles formed [82]. No variation was seen in the microstructure or microhardness over the entire 100 mm long, 6 mm tall deposition, and the average hardness was significantly lower than that of the feedstock (~80 HV compared to 120 HV). Tensile tests also showed that the as-deposited material had lower yield strength and ultimate tensile strength (UTS) compared to the feedstock; no deposition parameters were given in the paper. Further work by Anderson et al. examined tool rotational speed between 175 and 300 rpm, traverse feed rates of 88.9 and 137.9 mm/min, and feedstock feed rates of 88.9 and 101.6 mm/min, while the layer height was used as 1 mm [59]. The variations in grain size (6.2 to 8.8 μm) and hardness (75 to 82 HV) measured were small. The optimum parameter set was used to produce a large sample for tensile and fatigue test coupons; again, the measured tensile strength was low (UTS of 206 MPa) compared to the feedstock material (425 MPa). This was mainly attributed to the lack of precipitate strengthening in the deposited material. The fatigue life was also much lower than that seen for the wrought feedstock material [59] due to the lack of a post-deposition heat treatment. Beck et al. [83] studied the influence of a post-deposition heat treatment on the tensile strength of AA6061. Following a solution treatment at 296 °C and ageing at 80 °C, the samples exhibited grain growth, and needle-like β″ precipitates that were not present in the deposited material were observed. The deposited material exhibited a 47% reduction in tensile strength and, after the solution treatment and age (STA), the samples regained full wrought strength. Hahn et al. [58] studied the effect of STA on AA7050; following heat treatment, some sections had recrystalised into very large grains (~200 μm) while others retained the highly grain-refined structure typical of AFSD. Despite the very different microstructures of wrought plate and the AFSD samples following a STA, both conditions resulted in a tensile strength of ~495 MPa and a yield strength of 435 MPa compared to 330 MPa and 180 MPa for the as-deposited material (UTS and YS, respectively). These studies highlight the importance of a post-deposition heat treatment for precipitation strengthened aluminium alloys (such as AA2xxx, AA6xxx, and AA7xxx series alloys).

Phillips et al. undertook a design-of-experiments approach to the deposition of AA6061 by AFSD; the tool rotational speed was varied between 300 and 420 rpm, the feedstock feed rate varied between 66 and 122 mm/min, and the tool traverse feed varied between 127 and 229 mm/min [84]. It was found that a combination of low feedstock feed rate and high tool traverse speed produced depositions with voids and a lack of fusion, while the opposite conditions caused the formation of excessive flash. The grain size of the deposited material was reduced to 15 μm compared to 200 μm in the feedstock. Typically, smaller grain sizes lead to increased hardness; however, in this case the hardness was reduced due to the dissolution of precipitates as reported previously [85]. There was no significant difference in the microstructure of the various depositions, suggesting that for an AFSD microstructure, evolution is not process-dependant. In further work, Phillips et al. examined the influence of parallel overlapping tracks (6.35 mm overlap) deposited at 300 rpm and a traverse speed of 127 mm/min [86]. The feedstock feed rate was 69.9 mm/min and the overlapping return track used a slight reduction to compensate for the additional material (63.5 mm/min). Contamination by surface oxides were seen in the overlapping section; these have not been

reported in any other study on AFSD of aluminium alloys. In addition, the grain size was marginally smaller in the overlapping region compared to the middle of the deposition (9.1 and 10.6 μm, respectively). Tensile tests of samples taken across the overlap showed no reduction in strength or ductility compared to samples taken from the middle of the deposition. Ghadimi et al. [24] examined the influence of layer thickness on the tensile strength of AA6061. It was found that using 2 and 3 mm layer height produced higher tensile strength compared to 1 mm height; this was attributed to the difference in thermal history, although the deposition temperature was not measured. Again, samples taken from different positions in the X- and Y-plane showed no significant difference in tensile strength, as also shown by Phillips et al. [62] and Mason et al. [63]. Hartley et al. (2021) examined the deposition of AA6061-T6 onto 1.4 mm thick substrates of AA6022-T4 [16]. Depositions ranging between 0.9 and 2.54 mm thick were produced using varying operating conditions, with a flat-bottomed tool resulting in the best surface finish. A microstructural analysis showed an absence of defects and a reduced grain size (20 μm compared to 110 μm) and lower hardness level (70 HV compared to 115 HV), as reported in all studies on aluminium alloys so far. Due to the thermal gradient developed during the deposition and the very thin substrates used, high levels of distortion of the base plates were encountered upon removal of the clamps, with up to 9 mm over 150 mm length being measured [16]. Mason et al. found that the initial layers of the AA7050 alloy exhibited significant growth of the T-phase and S-phase, while η and η′ phases were absent in these layers. They reported that the overgrowth of strengthening precipitates in the initial and intermediate layers of each section caused material softening due to overaging. This overaging resulted from the repeated thermal cycles that the initial and intermediate layers underwent during AFSD processing [87].

Avery et al. used AA7075 feedstock manufactured by wire electro-discharge machining rods from billet material, and a single build 65 mm high by 102 mm long was deposited [81]. The tool rotational speed was 225 rpm, the material feed rate was 50.8 mm/min, and traverse feed rate was 50.8 mm/min, with each layer being 1 mm. The grain size was reduced from 100 μm to ~5 μm compared to the feedstock material and SEM analysis showed that the η′ and η precipitates that contribute to the high strength of the alloy have coarsened by repeated exposure to elevated temperatures during deposition. These microstructural changes led to a reduction in hardness, with a minimum of 60 HV compared to 175 HV for the feedstock. Due to the height of the build, a higher hardness was seen at the top of the build, with a peak hardness of 105 HV due to the reduced exposure to elevated temperatures. Tensile tests showed that the tensile and yield strength were reduced significantly compared to the feedstock material. Strain controlled fatigue tests also showed a reduction in fatigue life for the AFSD material compared to feedstock, and this was attributed to the precipitation coarsening seen in the microstructure [81]. Cahalan et al. [57] examined the influence of parallel deposition tracks and the amount of track overlap (going from 0 to 38%) on the resulting tensile strength of the AA7075 deposition. Tensile samples were taken in the horizontal direction across the overlap region and no post-deposition heat treatment was conducted. For overlaps greater than 3.2 mm, the boundary between the two tracks became indistinct and a high degree of intermixing had occurred. Tensile strength increased with an increase in overlap up to 38% (from 258 MPa to 434 MPa), and higher levels of overlap were not tested. Overlapping parallel tracks would be critical to produce larger surface area builds.

AFSD is also attractive for the repair or resurfacing of damaged or worn components. Griffiths et al. examined the ability of AFSD to repair holes and milled slots in AA7075 [30]. It was found that the holes could be filled in completely, with no lack of fusion defects or voids being seen. As reported previously, the microstructure was composed of extensively recrystallised equiaxed grains (down to 3.5 μm); in comparison to other work, the micro-hardness value of the deposited material is only slightly lower than the feedstock (140 HV compared to 175 HV) due to the shorter deposition time of the repair compared to bulk feature addition. One hole sample failed to completely fill, leaving a void at the bottom of

the hole. For the milled slots, all samples suffered from incomplete mixing and a lack of fusion. Griffiths et al. also examined the production of aluminium metal matrix composites (MMCs) using AFSD by taking aluminium and AA6061 feedstock rods and producing a hollow tube which was packed with various powder additions [30]. Three variations in feedstock were tested, namely aluminium with 20 vol.% silicon carbide (SiC), AA6061 with 30 vol.% molybdenum (Mo), and AA6061 with 6.1 vol% tungsten (W). For all variants, the samples produced contained a uniform distribution of particles and no defects could be seen in the depositions. Further work was undertaken by Lopez et al. to investigate the production of graphene nanoplatelet MMCs using AA6061 [88,89]. The results showed that it is possible to produce fully dense material without defects. When using a central bored section in the feedstock with mixed AA6061 powder and graphene nanoplatelets rather than just graphene alone, a better distribution of particles was obtained.

Magnesium (Mg) alloys have densities around 36% lower than aluminium alloys and are promising candidates for AFSD. Calvert investigated the deposition of Mg alloys with AFSD [44]; minor variations in grain size were seen with layer height due to the variation in thermal history but, in general, the deposition was uniform [44]. Williams et al. reported that Mg has a narrower processing window than aluminium alloys but found similar microstructural features with a highly refined grain structure (~2.7 μm compared to 45 μm for the feedstock) and lower hardness, tensile strength, and ductility compared to the wrought WE43 feedstock [42]. Joshi et al. also found that AZ31B deposited by AFSD had a highly refined grain structure (<5 μm) compared to the feedstock (~13.5 μm) but reported slightly higher hardness (~57 HV) than the feedstock (53 HV) due to the Hall-Patch effect [45]. In contrast, Robinson et al. reported the slightly lower hardness and tensile strength of AFSD AZ31B compared to the wrought feedstock [46].

For both aluminium alloys and magnesium alloys, the majority of reported work on AFSD shows that the as-deposited material has lower mechanical properties compared to wrought values. For nickel-based superalloys, the mechanical properties of as-deposited material have been shown to be comparable to wrought values. In a study on Inconel 625, Rivera et al. found the grain size of the deposited material to be reduced to 1 μm compared to the feedstocks, with sizes of 30 μm [39]. The deposited material also displayed a banded appearance, which was caused by the interface layers between each deposited layer having a slightly finer grain, around 0.25 μm. Tensile tests showed that the as-deposited AFSD material had higher yield strength and UTS compared to wrought and cast material, which is opposite to that seen for aluminium alloys [39]. In further work by Avery et al., it was found that the severe plastic deformation encountered in the shear zone caused the M23C6 and M6C carbides to be broken up into smaller size fractions and distributed more finely than in the feedstock material [40]. Fatigue tests showed that the AFSD samples exhibited higher fatigue life than the feedstock material, laser additively produced samples, and cast Inconel 625 samples. The improvement in fatigue life is attributed to the refinement in grain size and carbide size and distribution. Some delamination of interlayers was observed during testing, causing two samples to fail at very low cycles; no deposition parameters were given in the paper [40].

Titanium alloys are widely used in the aerospace industry in both structural and for engine components. In contrast to aluminium alloys, very few studies on titanium alloys have been undertaken. Agrawal et al. used feedstock manufactured from compacted Ti6Al4V metal swarf, three samples were produced using 1 mm layer thickness [37]. The AFSD process parameters employed in the study by Agrawal et al. are given in Table 2.

Table 2. Parameters used for depositing Ti6Al4V using AFSD process [37].

Sample No.	Number of Layers	Average Track Width (mm)	Average Power (kW)	Tool Rotational Rate (ω, rpm)	Traverse Speed (V, mm per min.)	Filler Rate (F, mm per min.)
B1	19	30.48	3.99	340	127	44.70
B2	39	35.56	5.59	325	86.36	40.39
B3	23	45.72	7.10	350	78.74	41.91

XRD scans showed that the microstructure consisted of α phase with a small amount of β phase, indicating that the operating temperature developed exceeded the β-transus. In contrast to studies on other materials (such as aluminium alloys), the influence of processing parameters was significant, and a variation was seen in grain size between the different builds and with build height [37]. For the highest tool rpm and lowest traverse feed rate, a grain size of 64 µm was seen; for the lower tool rpm and higher traverse feed rates, grain sizes of 26 and 30 µm were observed. Due to the temperatures developed during processing, a tungsten carbide (WC) tool is used; contamination caused by wear to the tool was seen in the interface layers of the builds, and subsequent tensile testing showed anisotropic behaviour, with the build direction having a lower yield strength compared to the horizontal direction (1060 and 1220 MPa) due to the formation of W phase in the interface layers [37]. Similar results were found by Farabi et al., who reported a yield strength of 1010 MPa and, by using a lanthannated-tungsten tool, prevented the contamination seen by Agrawal et al. [41]. Yoder et al. used a closed loop temperature control to keep the deposition temperature constant; in contrast to Agrawal et al. and Farabi et al., the microstructure grain size was constant throughout the height of the build and no variation in microhardness was seen [90]. The yield strength was slightly lower than the previous studies, at 948 MPa. As found with nickel-based superalloys, the as-deposited mechanical properties of Ti-6Al-4V are superior to other AM processes and approach that of wrought material [90].

Priedeman et al. studied the deposition of a copper alloy (Alloy Cu 110) at a tool rotational speed of 275 rpm and a traverse speed of 127 mm/min; no other parameters were given [47]. Some porosity was seen the interface between the substrate and the first layer. Oxidation was also seen on the outer surfaces of the deposit, but none in the interior, suggesting that the oxide layer had formed during cooling after deposition. As reported for a range of other materials, the grain size and hardness of the deposition were lower than that for the feedstock due to dynamic recrystallization (63 to 102 HV) [47]. Griffiths et al. (2021) also reported similar findings for Cu 110, except for one parameter combination using high tool rotational speed (600 rpm) combined with high traverse feed (parameters not given), in which the grain size was increased compared to that of the feedstock [17].

In summary, the typical microstructure obtained from AFSD is equiaxed and highly grain-refined, with lower mechanical strength compared to the wrought feedstock material with the notable exceptions of work on Ti6Al4V and Inconel 625, where the mechanical properties were equivalent to those of wrought as-deposited material. AFSD can produce large-scale bulk additive parts that do not suffer from the typical defects of fusion-based AM in materials that cannot be processed by other AM methods.

7. Summary

This review paper on AFSD aimed at demonstrating a systematic and comprehensive literature review to highlight the potential of this emerging AM technology while addressing the limitations and encountered challenges, together with possible technological solutions. The main conclusions to derive from this literature survey can be summarised as follows:

- AFSD is an emerging solid-state non-fusion AM technology with several benefits, especially for large-scale part manufacturing, to replace castings or forgings with long-lead times.
- Aluminium alloys are by far the most studied alloy group, with a range of AA2xxx, AA6xxx and AA7xxx alloys. There are some studies on stainless steels, Mg alloys, tool steels, and Ti6Al4V, but to expand the available material range, further research is needed.
- Defect-free part manufacturing in AFSD is highly dependent on the proper construction of process windows, with the most-studied key process variables being layer height, spindle speed, traverse speed, and actuator feed. For some materials, the process windows can be quite large, making the process development easier, whereas for more demanding materials such as high-strength Al alloys, the process windows are narrower.
- Unlike other additive manufacturing technologies based on fusion, AFSD achieves fully dense material when the process parameters are appropriately selected and issues such as a lack of fusion and keyhole porosities are avoided. The excessive flash regions on the sides of the deposited material, which are more prone to defects, need to be machined to reach the final geometry.
- The in situ monitoring of the process primarily consists of measuring temperature, force, torque, and acoustic emission levels. As a future direction, greater effort should be made to use closed-loop control instead of simply gathering the related data and only monitoring.
- Although there are limited process-modelling studies on this specific topic, research on similar processes such as friction stir welding is more prevalent than research on AFSD.
- Research on advanced mechanical properties such as fatigue or creep are mostly lacking for the alloys addressed so far, such as high-strength Al alloys. It is also clear that the range of available materials needs to be widened by determining process windows for other alloys.
- Finally, it is necessary to implement effective process modelling and simulation methods that can be executed using commonly utilised analysis software, in order to make it accessible to a wide range of researchers.

Funding: This research received no external funding.

Data Availability Statement: The data presented in this study are available on request from the corresponding author.

Conflicts of Interest: The authors declare no conflicts of interest.

References

1. Bourell, D.L.; Frazier, W.; Kuhn, H.; Seifi, M. *ASM Handbook®. Additive Manufacturing Processes*; ASM International: Materials Park, OH, USA, 2020.
2. Pei, E.; Kabir, I.R.; Leutenecker-Twelsiek, B. History of AM. In *Springer Handbook of Additive Manufacturing*; Springer International Publishing: Cham, Switzerland, 2023; pp. 3–29.
3. Khodabakhshi, F.; Gerlich, A.P. Potentials and strategies of solid-state additive friction-stir manufacturing technology: A critical review. *J. Manuf. Process.* **2018**, *36*, 77–92. [CrossRef]
4. Gibson, I.; Rosen, D.W.; Stucker, B.; Khorasani, M.; Rosen, D.; Stucker, B.; Khorasani, M. *Additive Manufacturing Technologies*; Springer: Cham, Switzerland, 2021; Volume 17, pp. 160–186.
5. Dilip, J.J.S.; Rafi, H.K.; Ram, G.D.J. A new additive manufacturing process based on friction deposition. *Trans. Indian Inst. Met.* **2011**, *64*, 27–30. [CrossRef]
6. Mishra, R.S.; Ma, Z.Y. Friction stir welding and processing. *Mater. Sci. Eng. R Rep.* **2005**, *50*, 1–78. [CrossRef]
7. Karthik, G.M.; Ram, G.J.; Kottada, R.S. Friction deposition of titanium particle reinforced aluminum matrix composites. *Mater. Sci. Eng. A* **2016**, *653*, 71–83. [CrossRef]
8. Elfishawy, E.; Ahmed, M.M.Z.; El-Sayed Seleman, M.M. Additive manufacturing of aluminum using friction stir deposition. In *TMS 2020 149th Annual Meeting & Exhibition Supplemental Proceedings*; Springer International Publishing: Berlin/Heidelberg, Germany, 2020; pp. 227–238.

9. Griffiths, R.J.; Petersen, D.T.; Garcia, D.; Yu, H.Z. Additive Friction Stir-Enabled Solid-State Additive Manufacturing for the Repair of 7075 Aluminum Alloy. *Appl. Sci.* **2019**, *9*, 3486. [CrossRef]
10. Martin, L.P.; Luccitti, A.; Walluk, M. Repair of aluminum 6061 plate by additive friction stir deposition. *Int. J. Adv. Manuf. Technol.* **2021**, *118*, 759–773. [CrossRef]
11. Yu, H.Z.; Mishra, R.S. Additive Friction Stir Deposition: A Deformation Processing Route to Metal Additive Manufacturing. *Mater. Res. Lett.* **2021**, *9*, 71–83. [CrossRef]
12. Merritt, G.R.; Williams, M.B.; Allison, P.G.; Jordon, J.B.; Rushing, T.W.; Cousin, C.A. Closed-Loop Temperature and Force Control of Additive Friction Stir Deposition. *J. Manuf. Mater. Process.* **2022**, *6*, 92. [CrossRef]
13. Garcia, D.; Hartley, W.D.; Rauch, H.A.; Griffiths, R.J.; Wang, R.; Kong, Z.J.; Zhu, Y.; Yu, H.Z. In situ investigation into temperature evolution and heat generation during additive friction stir deposition: A comparative study of Cu and Al-Mg-Si. *Addit. Manuf.* **2020**, *34*, 101386. [CrossRef]
14. Fehrenbacher, A.; Schmale, J.R.; Zinn, M.R.; Pfefferkorn, F.E. Measurement of Tool-Workpiece Interface Temperature Distribution in Friction Stir Welding. *J. Manuf. Sci. Eng.* **2014**, *136*, 021009. [CrossRef]
15. Mishra, R.S.; Haridas, R.S.; Agrawal, P. Friction Stir-based Additive Manufacturing. *Sci. Technol. Weld. Join.* **2022**, *27*, 141–165. [CrossRef]
16. Hartley, W.D.; Garcia, D.; Yoder, J.K.; Poczatek, E.; Forsmark, J.H.; Luckey, S.G.; Dillard, D.A.; Hang, Z.Y. Solid-State Cladding on Thin Automotive Sheet Metals Enabled by Additive Friction Stir Deposition. *J. Mater. Processing Technol.* **2021**, *291*, 117045. [CrossRef]
17. Griffiths, R.J.; Garcia, D.; Song, J.; Vasudevan, V.K.; Steiner, M.A.; Cai, W.; Hang, Z.Y. Solid-State Additive Manufacturing of Aluminum and Copper Using Additive Friction Stir Deposition: Process-Microstructure Linkages. *Materialia* **2021**, *15*, 100967. [CrossRef]
18. Gopan, V.; Wins, K.L.D.; Surendran, A. Innovative potential of additive friction stir deposition among current laser based metal additive manufacturing processes: A review. *CIRP J. Manuf. Sci. Technol.* **2021**, *32*, 228–248. [CrossRef]
19. Zhang, Z.; Tan, Z.J.; Li, J.Y.; Zu, Y.F.; Liu, W.W.; Sha, J.J. Experimental and numerical studies of re-stirring and re-heating effects on mechanical properties in friction stir additive manufacturing. *Int. J. Adv. Manuf. Technol.* **2019**, *104*, 767–784. [CrossRef]
20. Stubblefield, G.G.; Fraser, K.; Phillips, B.J.; Jordon, J.B.; Allison, P.G. A meshfree computational framework for the numerical simulation of the solid-state additive manufacturing process, additive friction stir-deposition (AFS-D). *Mater. Des.* **2021**, *202*, 109514. [CrossRef]
21. Jin, Y.; Yang, T.; Wang, T.; Dowden, S.; Neogi, A.; Dahotre, N.B. Behavioral Simulations and Experimental Evaluations of Stress Induced Spatial Nonuniformity of Dynamic Bulk Modulus in Additive Friction Stir Deposited AA 6061. *J. Manuf. Process.* **2023**, *94*, 454–465. [CrossRef]
22. Elshaghoul, Y.G.Y.; Seleman, M.M.E.-S.; Bakkar, A.; Elnekhaily, S.A.; Albaijan, I.; Ahmed, M.M.Z.; Abdel-Samad, A.; Reda, R. Additive Friction Stir Deposition of AA7075-T6 Alloy: Impact of Process Parameters on the Microstructures and Properties of the Continuously Deposited Multilayered Parts. *Appl. Sci.* **2023**, *13*, 10255. [CrossRef]
23. Ahmed, M.M.Z.; Seleman, M.M.E.-S.; Elfishawy, E.; Alzahrani, B.; Touileb, K.; Habba, M.I.A. The Effect of Temper Condition and Feeding Speed on the Additive Manufacturing of AA2011 Parts Using Friction Stir Deposition. *Materials* **2021**, *14*, 6396. [CrossRef]
24. Ghadimi, H.; Talachian, M.; Ding, H.; Emanet, S.; Guo, S. The Effects of Layer Thickness on the Mechanical Properties of Additive Friction Stir Deposition-Fabricated Aluminum Alloy 6061 Parts. *Metals* **2024**, *14*, 101. [CrossRef]
25. Tang, W.; Yang, X.; Tian, C. Influence of Rotation Speed on Interfacial Bonding Mechanism and Mechanical Performance of Aluminum 6061 Fabricated by Multilayer Friction-based Additive Manufacturing. *Int. J. Adv. Manuf. Technol.* **2023**, *126*, 4119–4133. [CrossRef]
26. Yakubov, V.; Ostergaard, H.; Bhagavath, S.; Leung, C.L.A.; Hughes, J.; Yasa, E.; Khezri, M.; Löschke, S.K.; Li, Q.; Paradowska, A.M. Recycled aluminium feedstock in metal additive manufacturing: A state of the art review. *Heliyon* **2024**, *10*, e27243. [CrossRef] [PubMed]
27. Agrawal, P.; Haridas, R.S.; Yadav, S.; Thapliyal, S.; Dhal, A.; Mishra, R.S. Additive friction stir deposition of SS316: Effect of process parameters on microstructure evolution. *Mater. Charact.* **2023**, *195*, 112470. [CrossRef]
28. Chen, G.; Wu, K.; Wang, Y.; Zhu, Z.; Nie, P.; Hu, F. Effect of rotational speed and feed rate on microstructure and mechanical properties of 6061 aluminum alloy manufactured by additive friction stir deposition. *Int. J. Adv. Manuf. Technol.* **2023**, *127*, 1165–1176. [CrossRef]
29. Mendieta, L.E.U.; Poyraz, O.; Yasa, E.; Hughes, J. An Experimental and Numerical Study on the Additive Friction Stir Deposition of Al 6061. In Proceedings of the AMC Turkey 2024, Antalya, Turkiye, 25–27 April 2024.
30. Griffiths, R.J.; Perry, M.E.J.; Sietins, J.M.; Zhu, Y.; Hardwick, N.; Cox, C.D.; Rauch, H.A.; Yu, H.Z. A Perspective on Solid-State Additive Manufacturing of Aluminum Matrix Composites Using MELD. *J. Mater. Eng. Perform.* **2018**, *28*, 648–656. [CrossRef]
31. Yoder, J.K.; Griffiths, R.J.; Yu, H.Z. Deformation-based additive manufacturing of 7075 aluminum with wrought-like mechanical properties. *Mater. Des.* **2021**, *198*, 109288. [CrossRef]
32. Perry, M.E.; Griffiths, R.J.; Garcia, D.; Sietins, J.M.; Zhu, Y.; Hang, Z.Y. Morphological and Microstructural Investigation of the Non-Planar Interface Formed in Solid-State Metal Additive Manufacturing by Additive Friction Stir Deposition. *Addit. Manuf.* **2020**, *35*, 101293. [CrossRef]

33. Williams, M.B.; Zhu, N.; Palya, N.I.; Hoarston, J.B.; McDonnell, M.M.; Kelly, M.R.; Lalonde, A.D.; Brewer, L.N.; Jordon, J.B.; Allison, P.G. Towards Understanding the Relationships between Processing Conditions and Mechanical Performance of the Additive Friction Stir Deposition Process. *Metals* **2023**, *13*, 1663. [CrossRef]
34. Chen, G.; Wu, K.; Wang, Y.; Sun, W.; Zhu, Z.; Lin, Y.; Hu, F. Numerical and Experimental Study on the Temperature Field of Additive Friction Stir Deposition. In Proceedings of the 2023 5th International Conference on Robotics and Computer Vision (ICRCV), Nanjing, China, 15–17 September 2023; pp. 266–270.
35. Hu, F.; Chen, G.; Lin, Y.; Wang, H.; Zhu, Z. Numerical and experimental study on the thermal process during additive friction stir deposition. *CIRP J. Manuf. Sci. Technol.* **2024**, *48*, 55–66. [CrossRef]
36. Kincaid, J.; Charles, E.; Garcia, R.; Dvorak, J.; No, T.; Smith, S.; Schmitz, T. Process planning for hybrid manufacturing using additive friction stir deposition. *Manuf. Lett.* **2023**, *37*, 26–31. [CrossRef]
37. Agrawal, P.; Haridas, R.S.; Yadav, S.; Thapliyal, S.; Gaddam, S.; Verma, R.; Mishra, R.S. Processing-Structure-Property Correlation in Additive Friction Stir Deposited Ti6Al4V Alloy from Recycled Metal Chips. *Addit. Manuf.* **2021**, *47*, 102259.
38. Patil, S.M.; Krishna, K.M.; Sharma, S.; Joshi, S.S.; Radhakrishnan, M.; Banerjee, R.; Dahotre, N.B. Thermo-Mechanical Process Variables Driven Microstructure Evolution During Additive Friction Stir Deposition of IN625. *Addit. Manuf.* **2024**, *80*, 103958. [CrossRef]
39. Rivera, O.G.; Allison, P.G.; Jordon, J.B.; Rodriguez, O.L.; Brewer, L.N.; McClelland, Z.; Whittington, W.R.; Francis, D.; Su, J.; Martens, R.L.; et al. Microstructures and mechanical behavior of Inconel 625 fabricated by solid-state additive manufacturing. *Mater. Sci. Eng. A* **2017**, *694*, 1–9. [CrossRef]
40. Avery, D.Z.; Rivera, O.G.; Mason, C.J.T.; Phillips, B.J.; Jordon, J.B.; Su, J.; Allison, P.G. Fatigue Behavior of Solid-State Additive Manufactured Inconel 625. *Jom* **2018**, *70*, 2475–2484. [CrossRef]
41. Farabi, E.; Babaniaris, S.; Barnett, M.R.; Fabijanic, D.M. Microstructure and mechanical properties of Ti6Al4V alloys fabricated by additive friction stir deposition. *Addit. Manuf. Lett.* **2022**, *2*, 100034. [CrossRef]
42. Williams, M.B.; Robinson, T.W.; Williamson, C.J.; Kinser, R.P.; Ashmore, N.A.; Allison, P.G.; Jordon, J.B. Elucidating the Effect of Additive Friction Stir Deposition on The Resulting Microstructure and Mechanical Properties of Magnesium Alloy we43. *Metals* **2021**, *11*, 1739. [CrossRef]
43. Luo, T.; Tang, W.; Wang, R.; Wang, S.; Xiao, L.; Yang, X. Microstructure heterogeneity and mechanical properties of Mg-Gd-Y-Zr alloy fabricated by force-controlled additive friction stir deposition. *Mater. Lett.* **2023**, *340*, 134164. [CrossRef]
44. Calvert, J.R. Microstructure and Mechanical Properties of WE43 Alloy Produced via Additive Friction Stir Technology. Doctoral Dissertation, Virginia Tech, Blacksburg, VA, USA, 2015.
45. Joshi, S.S.; Patil, S.M.; Mazumder, S.; Sharma, S.; Riley, D.A.; Dowden, S.; Banerjee, R.; Dahotre, N.B. Additive friction stir deposition of AZ31B magnesium alloy. *J. Magnes. Alloy.* **2022**, *10*, 2404–2420. [CrossRef]
46. Robinson, T.; Williams, M.; Rao, H.; Kinser, R.P.; Allison, P.G.; Jordon, J.B. Microstructural and Mechanical Properties of a Solid-State Additive Manufactured Magnesium Alloy. *J. Manuf. Sci. Eng.* **2022**, *144*, 061013. [CrossRef]
47. Priedeman, J.L.; Phillips, B.J.; Lopez, J.J.; Roper, B.E.T.; Hornbuckle, B.C.; Darling, K.A.; Jordon, J.B.; Allison, P.G.; Thompson, G.B. Microstructure Development in Additive Friction Stir-Deposited Cu. *Metals* **2020**, *10*, 1538. [CrossRef]
48. Jordon, J.B.; Allison, P.G.; Phillips, B.J.; Avery, D.Z.; Kinser, R.P.; Brewer, L.N.; Cox, C.; Doherty, K. Direct Recycling of Machine Chips Through a Novel Solid-State Additive Manufacturing Process. *Mater. Des.* **2020**, *193*, 108850. [CrossRef]
49. Shao, J.; Samaei, A.; Xue, T.; Xie, X.; Guo, S.; Cao, J.; MacDonald, E.; Gan, Z. Additive friction stir deposition of metallic materials: Process, structure and properties. *Mater. Des.* **2023**, *234*, 112356. [CrossRef]
50. Schröder, J.; Evans, A.; Luzin, V.; Faria, G.A.; Degener, S.; Polatidis, E.; Čapek, J.; Kromm, A.; Dovzhenko, G.; Bruno, G. Texture-based residual stress analysis of laser powder bed fused Inconel 718 parts. *J. Appl. Crystallogr.* **2023**, *56*, 1076–1090. [CrossRef] [PubMed]
51. Szost, B.A.; Terzi, S.; Martina, F.; Boisselier, D.; Prytuliak, A.; Pirling, T.; Hofmann, M.; Jarvis, D.J. A comparative study of additive manufacturing techniques: Residual stress and microstructural analysis of CLAD and WAAM printed Ti–6Al–4V components. *Mater. Des.* **2016**, *89*, 559–567. [CrossRef]
52. Yakubov, V.; Ostergaard, H.; Hughes, J.; Yasa, E.; Karpenko, M.; Proust, G.; Paradowska, A.M. Evolution of Material Properties and Residual Stress with Increasing Number of Passes in Aluminium Structure Printed via Additive Friction Stir Deposition. *Materials* **2024**, *17*, 3457. [CrossRef]
53. Zhu, N.; Avery, D.Z.; Chen, Y.; An, K.; Jordon, J.B.; Allison, P.G.; Brewer, L.N. Residual Stress Distributions in AA6061 Material Produced by Additive Friction Stir Deposition. *J. Mater. Eng. Perform.* **2023**, *32*, 5535–5544. [CrossRef]
54. Yu, H.Z.; Jones, M.E.; Brady, G.W.; Griffiths, R.J.; Garcia, D.; Rauch, H.A.; Cox, C.D.; Hardwick, N. Non-beam-based metal additive manufacturing enabled by additive friction stir deposition. *Scr. Mater.* **2018**, *153*, 122–130. [CrossRef]
55. Tang, W.; Yang, X.; Tian, C.; Gu, C. Effect of rotation speed on microstructure and mechanical anisotropy of Al-5083 alloy builds fabricated by friction extrusion additive manufacturing. *Mater. Sci. Eng. A* **2022**, *860*, 144237. [CrossRef]
56. Turner, B.N.; Gold, S.A. A review of melt extrusion additive manufacturing processes: II. Materials, dimensional accuracy, and surface roughness. *Rapid Prototyp. J.* **2015**, *21*, 250–261. [CrossRef]
57. Cahalan, L.P.; Williams, M.B.; Brewer, L.N.; McDonnell, M.M.; Kelly, M.R.; Lalonde, A.D.; Allison, P.G.; Jordon, J.B. Parametric Investigation of Parallel Deposition Passes on the Microstructure and Mechanical Properties of 7075 Aluminum Alloy Processed with Additive Friction Stir Deposition. *Appl. Sci.* **2024**, *14*, 457. [CrossRef]

58. Hahn, G.D.; Knight, K.P.; Gotawala, N.; Hang, Z.Y. Additive Friction Stir Deposition of AA7050 Achieving Forging-Like Tensile Properties. *Mater. Sci. Eng. A* **2024**, *896*, 146268. [CrossRef]
59. Anderson-Wedge, K.; Avery, D.Z.; Daniewicz, S.R.; Sowards, J.W.; Allison, P.G.; Jordon, J.B.; Amaro, R.L. Characterization of the fatigue behavior of additive friction stir-deposition AA2219. *Int. J. Fatigue* **2021**, *142*, 105951. [CrossRef]
60. Gumaste, A.; Dhal, A.; Agrawal, P.; Haridas, R.S.; Vasudevan, V.K.; Weiss, D.; Mishra, R.S. A Novel Approach for Enhanced Mechanical Properties in Solid-State Additive Manufacturing by Additive Friction Stir Deposition Using Thermally Stable Al-Ce-Mg Alloy. *JOM* **2023**, *75*, 4185–4198. [CrossRef]
61. Beladi, H.; Farabi, E.; Hodgson, P.D.; Barnett, M.R.; Rohrer, G.S.; Fabijanic, D. Microstructure evolution of 316L stainless steel during solid-state additive friction stir deposition. *Philos. Mag.* **2021**, *102*, 618–633. [CrossRef]
62. Mishra, D.; Gupta, A.; Raj, P.; Kumar, A.; Anwer, S.; Pal, S.K.; Chakravarty, D.; Pal, S.; Chakravarty, T.; Pal, A.; et al. Real time monitoring and control of friction stir welding process using multiple sensors. *CIRP J. Manuf. Sci. Technol.* **2020**, *30*, 1–11. [CrossRef]
63. Everton, S.K.; Hirsch, M.; Stravroulakis, P.; Leach, R.K.; Clare, A.T. Review of in-situ process monitoring and in-situ metrology for metal additive manufacturing. *Mater. Des.* **2016**, *95*, 431–445. [CrossRef]
64. Liu, X.C.; Sun, Y.F.; Nagira, T.; Ushioda, K.; Fujii, H. Experimental evaluation of strain and strain rate during rapid cooling friction stir welding of pure copper. *Sci. Technol. Weld. Join.* **2019**, *24*, 352–359. [CrossRef]
65. Chaudhary, B.; Jain, N.K.; Murugesan, J.; Patel, V. Exploring temperature-controlled friction stir powder additive manufacturing process for multi-layer deposition of aluminum alloys. *J. Mater. Res. Technol.* **2022**, *20*, 260–268. [CrossRef]
66. Chaudhary, B.; Patel, V.; Ramkumar, P.L.; Vora, J. Temperature Distribution During Friction Stir Welding of AA2014 Aluminum Alloy: Experimental and Statistical Analysis. *Trans. Indian Inst. Met.* **2019**, *72*, 969–981. [CrossRef]
67. Assidi, M.; Fourment, L.; Guerdoux, S.; Nelson, T. Friction Model for Friction Stir Welding Process Simulation: Calibrations from Welding Experiments. *Int. J. Mach. Tools Manuf.* **2010**, *50*, 143–155. [CrossRef]
68. Swaminathan, S.; Oh-Ishi, K.; Zhilyaev, A.P.; Fuller, C.B.; London, B.; Mahoney, M.W.; McNelley, T.R. Peak Stir Zone Temperatures during Friction Stir Processing. *Met. Mater. Trans. A* **2010**, *41*, 631–640. [CrossRef]
69. Gerlich, A.; Avramovic-Cingara, G.; North, T.H. Stir zone microstructure and strain rate during Al 7075-T6 friction stir spot welding. *Met. Mater. Trans. A* **2006**, *37*, 2773–2786. [CrossRef]
70. Cunningham, R.; Zhao, C.; Parab, N.; Kantzos, C.; Pauza, J.; Fezzaa, K.; Sun, T.; Rollett, A.D. Keyhole threshold and morphology in laser melting revealed by ultrahigh-speed x-ray imaging. *Science* **2019**, *363*, 849–852. [CrossRef] [PubMed]
71. Yakubov, V.; Ostergaard, H.; Bhagavath, S.; Leung, C.L.A.; Hughes, J.; Yasa, E.; Khezri, M.; Loschke, S.K.; Li, Q.; Paradowska, A.M. Hardness distribution and defect formation in aluminium alloys fabricated via additive friction stir deposition (AFSD). In Proceedings of the 11th Australasian Congress on Applied Mechanics (ACAM2024), Brisbane, Australia, 7–9 February 2024.
72. Escobar, R., Jr.; Fraser, K.; Jordon, J.B.; Alison, P.G. Meshfree Simulation of Oxide Dispersion in Meld of Aluminum Alloys. In Proceedings of the 12th International Symposium on Friction Stir Welding, Saguenay, QC, Canada, 26–28 June 2018.
73. Zhang, Z.; Tan, Z.-J.; Li, J.-Y.; Zu, Y.-F.; Sha, J.-J. Integrated Modeling of Process–Microstructure–Property Relations in Friction Stir Additive Manufacturing. *Acta Met. Sin. (Engl. Lett.)* **2020**, *33*, 75–87. [CrossRef]
74. Shi, T.; Wu, J.; Ma, M.; Charles, E.; Schmitz, T. AFSD-Nets: A Physics-informed Machine Learning Model for Predicting the Temperature Evolution During Additive Friction Stir Deposition. *J. Manuf. Sci. Eng.* **2024**, *146*, 081003. [CrossRef]
75. Frigaard, Ø.; Grong, Ø.; Midling, O.T. A process model for friction stir welding of age hardening aluminum alloys. *Met. Mater. Trans. A* **2001**, *32*, 1189–1200. [CrossRef]
76. Coegrove, P. 3-Dimensional Flow and Thermal Modelling of the Friction Stir Welding Process. Doctoral Dissertation, University of Adelaide, Adelaide, Australia, 2001.
77. Song, M.; Kovacevic, R. Heat transfer modelling for both workpiece and tool in the friction stir welding process: A coupled model. *Proc. Inst. Mech. Eng. Part B J. Eng. Manuf.* **2004**, *218*, 17–33. [CrossRef]
78. Liechty, B.; Webb, B. Modeling the frictional boundary condition in friction stir welding. *Int. J. Mach. Tools Manuf.* **2008**, *48*, 1474–1485. [CrossRef]
79. Guerdoux, S. Numerical Simulation of The Friction Stir Welding Process. Doctoral Dissertation, École Nationale Supérieure des Mines de Paris, Paris, France, 2007.
80. Heuzéa, T.; Leblond, J.B.; Bergheau, J.M. Modelling of Fluid/Solid Couplings in High Temperature Assembly Processes: Application to The Friction Stir Spot Welding. In Proceedings of the 2nd International Conference on Friction Stir Welding and Processing (FSWP 2012), Saint-Etienne, France, 26–27 January 2012.
81. Avery, D.Z.; Phillips, B.J.; Mason, C.J.T.; Palermo, M.; Williams, M.B.; Cleek, C.; Rodriguez, O.L.; Allison, P.G.; Jordon, J.B. Influence of Grain Refinement and Microstructure on Fatigue Behavior for Solid-State Additively Manufactured Al-Zn-Mg-Cu Alloy. *Met. Mater. Trans. A* **2020**, *51*, 2778–2795. [CrossRef]
82. Rivera, O.G.; Allison, P.G.; Brewer, L.N.; Rodriguez, O.L.; Jordon, J.B.; Liu, T.; Whittington, W.R.; Martens, L.R.; McClelland, Z.; Mason, C.J.T.; et al. Influence of texture and grain refinement on the mechanical behavior of AA2219 fabricated by high shear solid state material deposition. *Mater. Sci. Eng. A* **2018**, *724*, 547–558. [CrossRef]
83. Beck, S.C.; Rutherford, B.A.; Avery, D.Z.; Phillips, B.J.; Rao, H.; Rekha, M.Y.; Brewer, L.N.; Allison, P.G.; Jordon, J.B. The effect of solutionizing and artificial aging on the microstructure and mechanical properties in solid-state additive manufacturing of precipitation hardened Al–Mg–Si alloy. *Mater. Sci. Eng. A* **2021**, *819*, 141351. [CrossRef]

84. Phillips, B.J.; Avery, D.Z.; Liu, T.; Rodriguez, O.L.; Mason, C.J.T.; Jordon, J.B.; Brewer, L.N.; Allison, P.G. Microstructure-Deformation Relationship of Additive Friction Stir-Deposition Al–Mg–Si. *Materialia* **2019**, *7*, 100387. [CrossRef]
85. Pariyar, A.; Yasa, E.; Sharman, A.; Guan, D. Investigations on the Solid-State Additive Manufacturing of Al Alloy: Process, Microstructure, and Crystallographic Texture. In *Light Metals 2024. TMS 2024*; Wagstaff, S., Ed.; The Minerals, Metals & Materials Series; Springer: Cham, Switzerland, 2024. [CrossRef]
86. Phillips, B.J.; Mason CJ, T.; Beck, S.C.; Avery, D.Z.; Doherty, K.J.; Allison, P.G.; Jordon, J.B. Effect of parallel deposition path and interface material flow on resulting microstructure and tensile behavior of Al-Mg-Si alloy fabricated by additive friction stir deposition. *J. Mech. Work. Technol.* **2021**, *295*, 117169. [CrossRef]
87. Mason, C.J.T.; Rodriguez, R.I.; Avery, D.Z.; Phillips, B.J.; Bernarding, B.P.; Williams, M.B.; Allison, P.G. Process-Structure-Property Relations for As-Deposited Solid-State Additively Manufactured High-Strength Aluminum Alloy. *Addit. Manuf.* **2021**, *40*, 101879. [CrossRef]
88. Lopez, J.J.; Williams, M.B.; Rushing, T.W.; Confer, M.P.; Ghosh, A.; Griggs, C.S.; Jordon, J.B.; Thompson, G.B.; Allison, P.G. A solid-state additive manufacturing method for aluminum-graphene nanoplatelet composites. *Materialia* **2022**, *23*, 101440. [CrossRef]
89. Lopez, J.J.; Williams, M.B.; Rushing, T.W.; Bikmukhametov, I.; Jordon, J.B.; Allison, P.G.; Thompson, G.B. Solid-state additive manufacturing of dispersion strengthened aluminum with graphene nanoplatelets. *Mater. Sci. Eng. A* **2024**, *893*, 146148. [CrossRef]
90. Yoder, J.K.; Erb, D.J.; Henderson, R.; Hang, Z.Y. Closed-loop temperature controlled solid-state additive manufacturing of Ti-6Al-4V with forging standard out-of-plane tensile properties. *J. Mater. Process. Technol.* **2023**, *322*, 118201. [CrossRef]